Novel materials for spintronics

鄭弘泰(Horng-Tay Jeng)
清華大學物理系

Mar 13, 2013, NTHU

Outline

- Spin and spintronics
- Theoretical background
- Magnetic materials
- Half-metal
- Multiferroic
- Topological insulator
- Spin polarized 2DEG
- Heterostructures
- Monolayers

Spin

- Stern–Gerlach experiment (1922)
- Pauli exclusion principle and Pauli (spinor) matrix (2x2), extra 2 state degree of freedom in addition to n,l,m (1924)
- Kronig, Uhlenbeck, Goudsmit call the extra degree of freedom as the electron spin (1925) (Pauli dislikes the name “spin”)
- Heisenberg matrix mechanics (1925)
- Schrödinger equation (1926)
- Fully relativistic Dirac spinor matrix (4x4) (1928)

Stern–Gerlach experiment (1922)

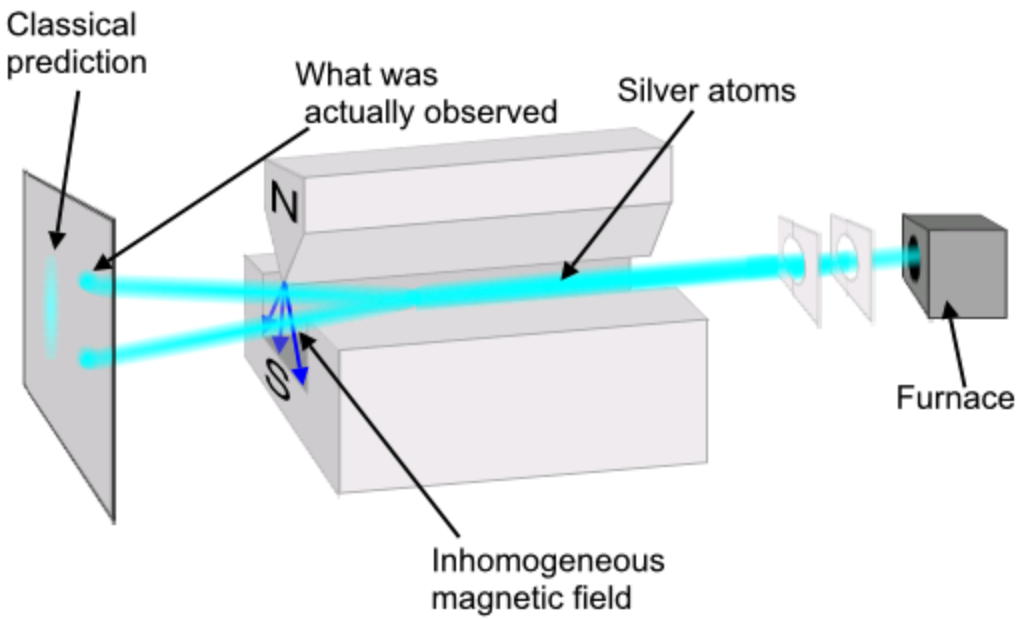

Spin electron

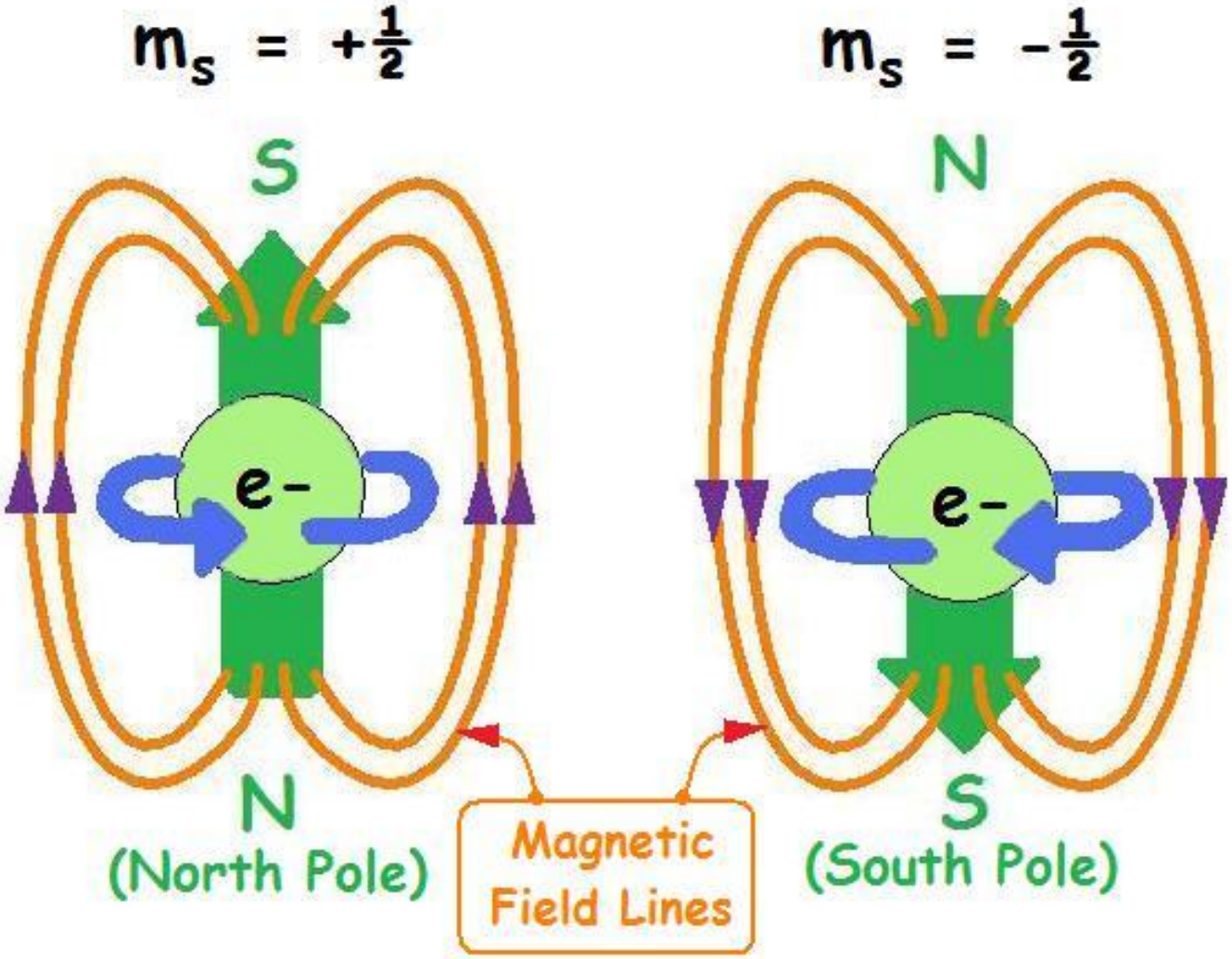

Spintronics

- Magnetoelectronics
- Spin transport electronics
- A new technology exploiting both the intrinsic spin of the electron and its associated magnetic moment, in addition to its fundamental electronic charge, in solid-state devices

Magnetite Fe3O4 磁鐵礦

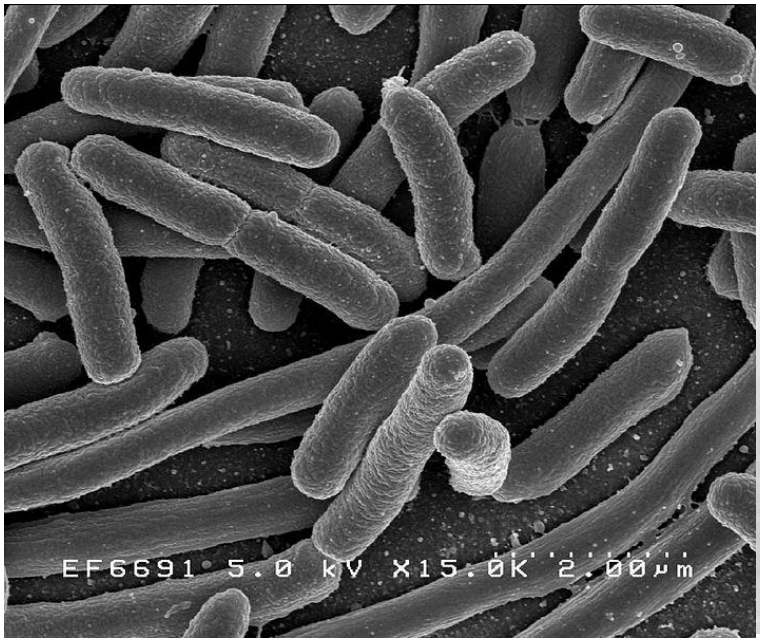

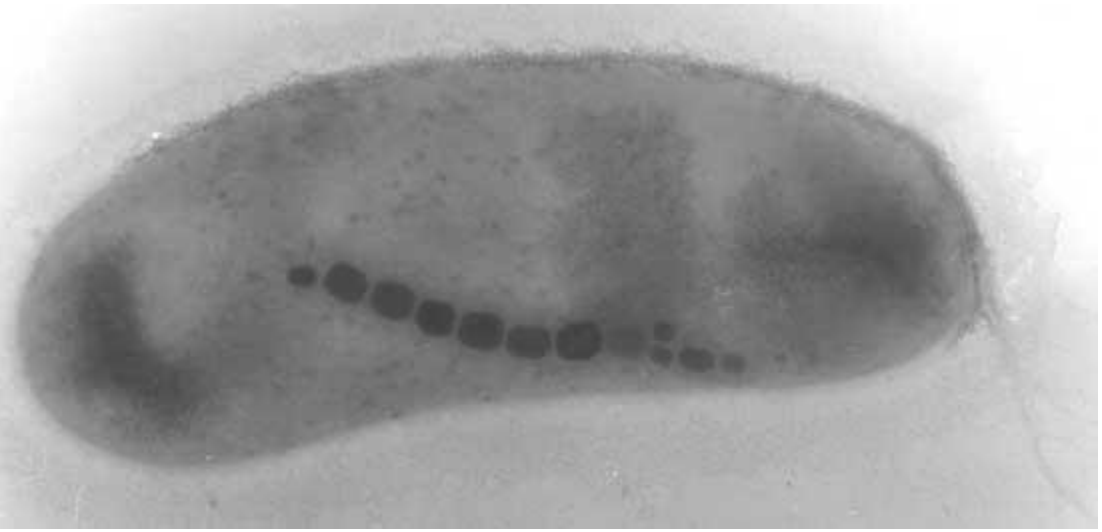

Actual TEM photo of a freshwater magnetotactic bacterium. The chain of dark objects are crystals of the mineral magnetite (Fe_3O_4), which have the proper size and shape to behave as perfect, single magnetic domains. The largest crystals are about 70 nm in length. *(Photo credit: A. Kobayashi)*.

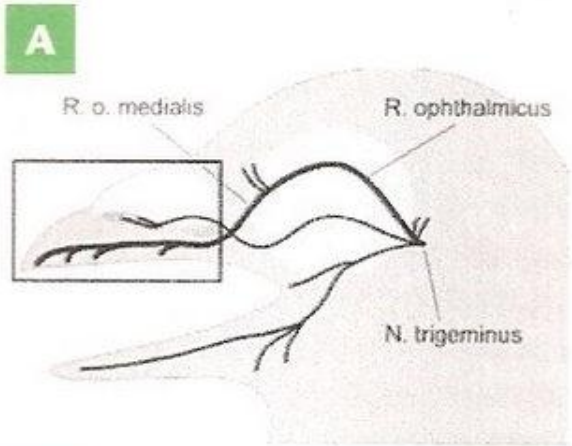
A
R. o. medialis
R. ophthalmicus
N. trigeminus

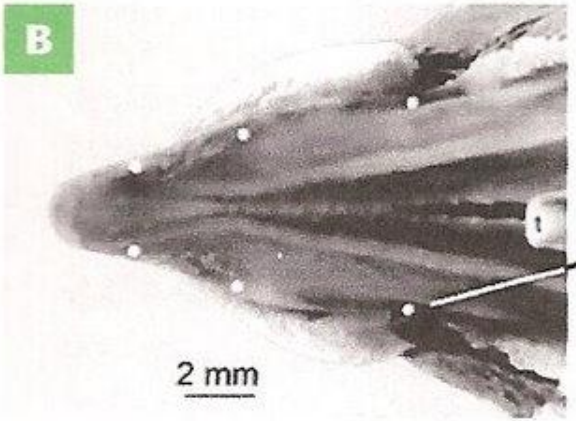
B
2 mm

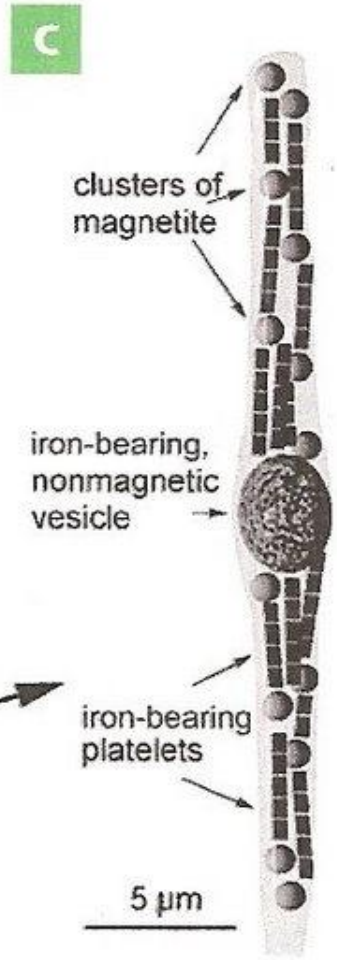
C
clusters of magnetite
iron-bearing, nonmagnetic vesicle
iron-bearing platelets
5 µm

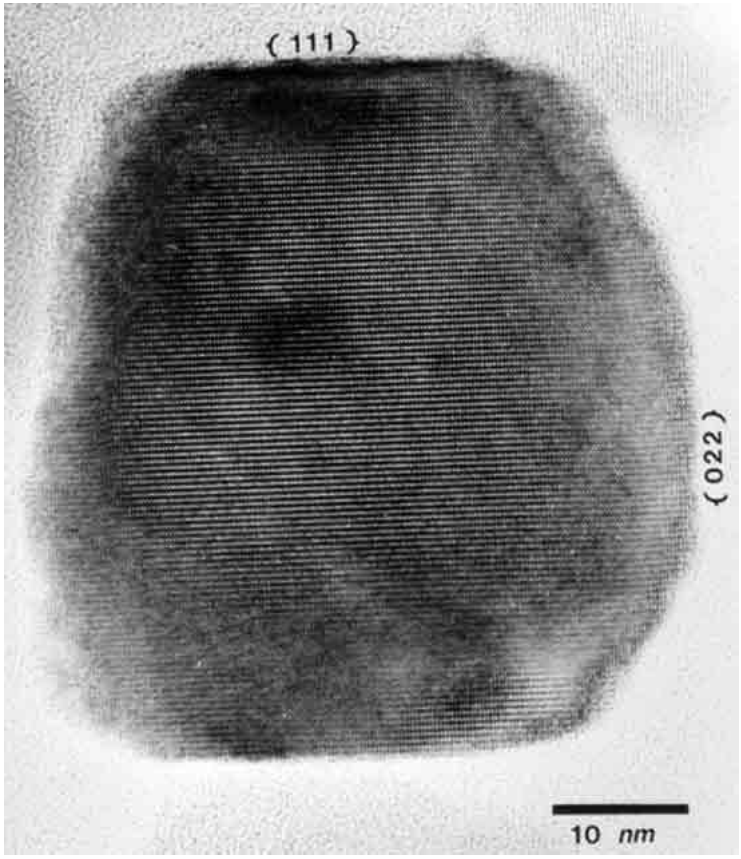

Above: High-resolution TEM image of a single-domain magnetite (Fe_3O_4) crystal from the human cerebellum. This image shows the pattern of intersecting {111} and {022} crystal lattice fringes, with particle elongation in the [111] lattice direction. The morphology and structure of these crystals resemble strongly those produced by the magnetotactic bacteria and salmon. Although biogenic magnetite is present in trace levels (1-100 ppb) in most human tissue samples, we do not yet know what biological function it has, if any.

Spin-dependent electron transport phenomena in solid-state devices: Emergence of spintronics (1980s)

- ferromagnet/superconductor tunneling experiments and magnetic tunnel junctions experiments (1970s).
- spin-polarized electron injection from a ferromagnetic metal to a normal metal (1985)
- giant magnetoresistance (GMR) (1988)
- theoretical proposal of a spin field-effect-transistor using semiconductors (1990)
- spin electrons persist for more than a nanosecond, longer than the modern processor clock cycle, electron spins available for information processing (IBM, 2012)

Properties desired for spintronics

- Magnetism
- Strong coupling between electron charge and spin
- Spin polarized current

Theoretical background

- First-Principles (第一原理):
- ***ab-initio (Latin)***
- **從頭開始** (Chinese)
- Start with Schrodinger-like equation without free adjusting parameter

Schrodinger equation+Hartree-Fock approximation

$$-\frac{\bar{h}^2}{2m}\nabla^2\psi(\vec{r})+V(\vec{r})\psi(\vec{r})=E\psi(\vec{r})$$

- Many-electron wavefunctions = Slater-determinants

$$\Psi^a_{\alpha_1\ldots\alpha_N}(q_1,\ldots,q_N)=\frac{1}{\sqrt{N!}}\begin{vmatrix}\phi_{\alpha_1}(q_1) & \cdots & \phi_{\alpha_1}(q_N)\\ \vdots & & \vdots\\ \phi_{\alpha_N}(q_1) & \cdots & \phi_{\alpha_N}(q_N)\end{vmatrix}$$

$$=\frac{1}{\sqrt{N!}}\sum_P(-1)^P P\phi_{\alpha_1}(q_1)\cdots\phi_{\alpha_N}(q_N)$$

Many-electron Hamiltonian

$$H=\sum_{i=1}^{N}\frac{p_i^2}{2m}+\sum_{i=1}^{N}V_{ext}(\vec{r})+\frac{1}{2}\sum_{i=1}^{N}\sum_{j=1(j\neq i)}^{N}\frac{e^2}{\left|\vec{r}_i-\vec{r}_j\right|}$$

Solvable up to 10~20 electrons(CI), almost impossible for solid.

Density Functional Theory (DFT)

Hohenberg-Kohn Theorem, PR136(1964)B864

- The ground-state energy of a system is a unique functional of the particle density.
- This functional attains its minimum value when the density has its correct values.

Local (spin) density approximation (L(S)DA)

Kohn-Sham scheme PR140(1965)A1133

$$E_G[n(\vec{r})] = T_S[n] + \int n(\vec{r}) V_{ext}(\vec{r}) d^3r$$

$$+ \frac{1}{2} \int \frac{n(\vec{r}) n(\vec{r}\,')}{|\vec{r} - \vec{r}\,'|} d^3r d^3r' + E_{xc}[n]$$

$$V(\vec{r}) = V_{ext}(\vec{r}) + \int d^3r' \frac{n(\vec{r}\,')}{|\vec{r} - \vec{r}\,'|} + V_{xc}[n(\vec{r})]$$

Total Energy of Fe

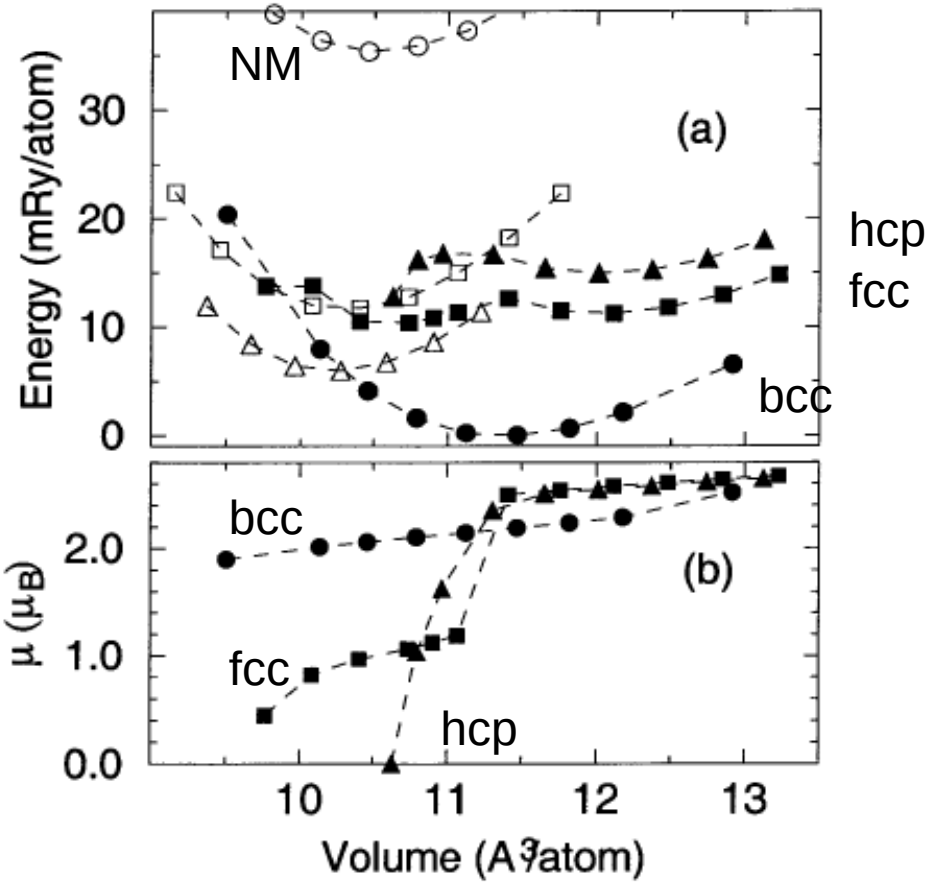

FIG. 1. (a) Total energy (relative to -2545.611 Ry/atom) of Fe as a function of volume per atom for bcc (circles), fcc (squares) and hcp (triangles). The curves are a polynomial fit to the total energies. Solid symbols denote the ferromagnetic states and open symbols, the nonmagnetic states. (b) Magnetic moment (μ) of bcc, fcc and hcp Fe as a function of volume per atom.

Slater-Pauling Curve: Experiment and LSDA Theory

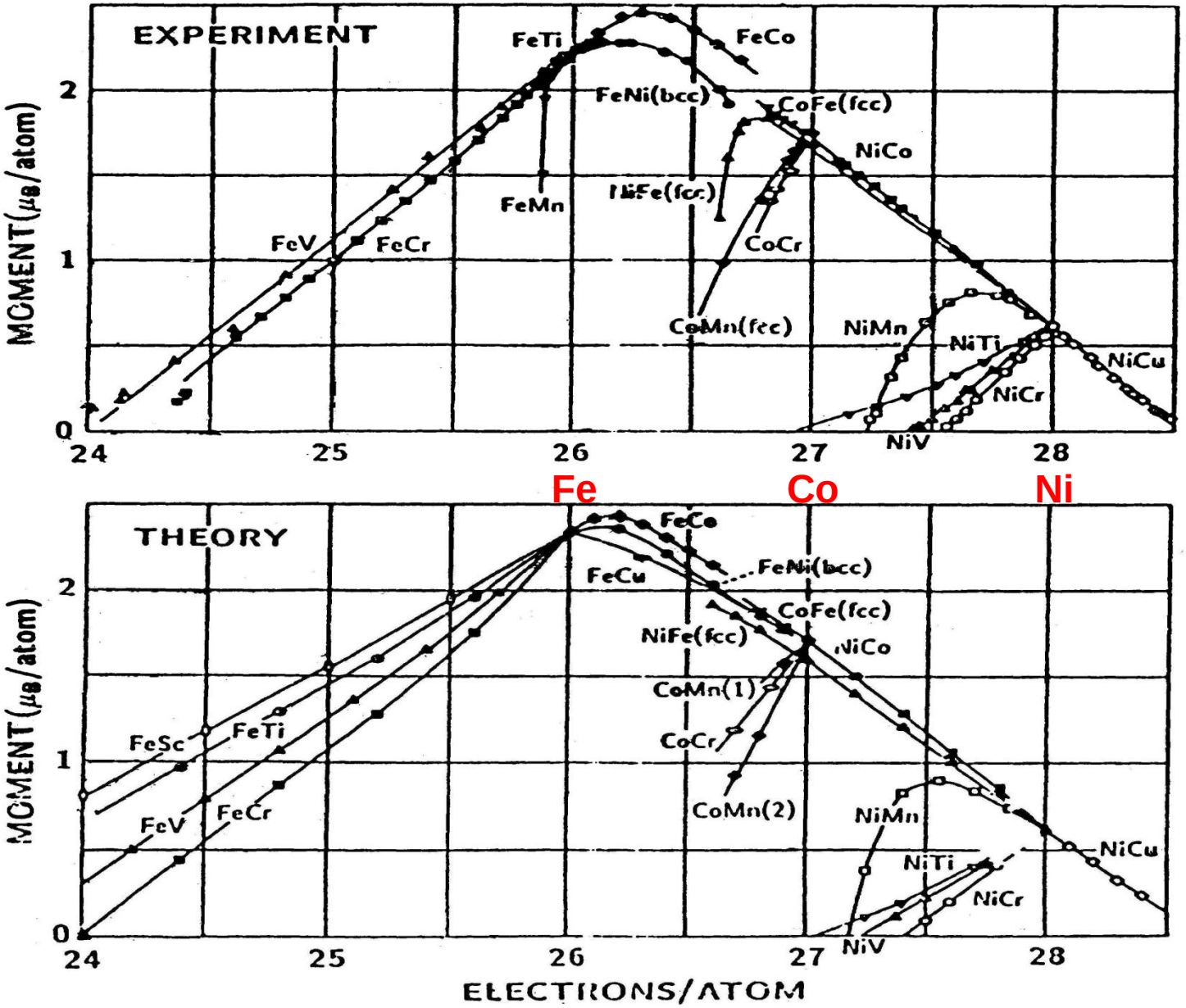

L(S)DA is very successful for weakly correlated systems!!

Insufficiencies of LDA

- Poor eigenvalues, PRB23, 5048 (1981)
- Lack of derivative discontinuity at integer N, PRL49, 1691 (1982)
- Gaps too small or no gap, PRB44, 943 (1991)
- Spin and orbital moment too small, PRB44, 943 (1991)
- Especially for transition metal oxides

TABLE II. Experimental (expt) and calculated (LDA + U) spin moments (m, in μ_B) and energy gaps (E, in eV) of the late-3d-transition-metal monoxides. For comparison, we also show these quantities as calculated from LSDA (Ref. 1).

	E_{LSD}	$E_{\mathrm{LSD}+U}$	E_{expt}	m_{LSD}	$m_{\mathrm{LSD}+U}$	m_{expt}
$CaCuO_2$	0.0	2.1	1.5[a]	0.0	0.66	0.51[b]
CuO	0.0	1.9	1.4[c]	0.0	0.74	0.65[d]
NiO	0.2	3.1	4.3,[e]4.0[f]	1.0	1.59	1.77,[9]1.64,[h]1.90[i]
CoO	0.0	3.2	2.4[j,k]	2.3	2.63 (3.60)	3.35,[l]3.8[m]
FeO	0.0	3.2	2.4[n]	3.4	3.62 (4.59)	3.32[m]
MnO	0.8	3.5	3.6–3.8[o]	4.4	4.61	4.79,[8]4.58[i]

[a]Y. Tokura, T. Arima, S. Koshihara, T. Ido, S. Ishibasi, H. Takagi, and S. Uchida, *Proceedings of the Second International Symposium on Superconductivty,* Tsukuba (Springer, New York, in press).
[b]D. Vaknin, E. Couignol, P. K. Devies, J. E. Fischer, D. C. Johnson, and D. P. Goshorn, Phys. Rev. B **39,** 9122 (1989).
[c]F. P. Koffyberg and F. A. B
[d]J. B. Forsyth, P. J. Brown, a
[e]G. A. Sawatzky and J. W. A
[f]S. Hüfner, J. Osterwalder, T.
[g]B. E. F. Fender, A. J. Jacob
[h]H. A. Alperin, J. Phys. Soc.
[i]A. K. Cheetham and D. A. C
[j]J. van Elp *et al.* (unpublished).
[k]R. J. Powell and W. E. Spicer, Phys. Rev. B **2,** 2182 (1970).
[l]D. C. Kahn and R. A. Ericson, Phys. Rev. B **1,** 2243 (1970).
[m]W. L. Roth, Phys. Rev. **110,** 1333 (1958); D. Hermann-Ronzaud, P. Burlet, and J. Rossat Mignod, J. Phys. C **11,** 2123 (1978).
[n]H. K. Bowen, D. Adler, and B. H. Auker, J. Solid State Chem. **12,** 355 (1975).
[o]R. N. Iskenderov, I. A. Drabkin, L. T. Emel'yanova, and Ya. Ksendzov, Fiz. Tverd. Tela (Leningrad) **10,** 2573 (1968) [Sov. Phys.—Solid State **10,** 2031 (1969)]; L. Messick, W. C. Walker, and R. Glosser, Phys. Rev. B **6,** 3941 (1972).

Gaps too small or no gap

Spin and orbital moment too small

PRB 44 (1991) 943

Beyond LDA

- Self-interaction correction (SIC) PRB23(1981)5048, PRL65(1990)1148
- Optimized effective potential method (OEP)
- Hartree-Fock (HF) method, PRB48(1993)5058
- GW approximation (GWA), PRB46(1992)13051, PRL74(1995)3221
- Time-dependent density functional theory (TDDFT)
- Dynamical mean field theory (DMFT)
- Quantum Monte-Carlo method (QMC)
- LDA+Hubbard U (LDA+U) method, PRB44(1991)943, PRB48(1993)16929

Local density approximation (LDA)

Kohn-Sham scheme PR140(1965)A1133

$$E_G[n(\vec{r})] = T_S[n] + \int n(\vec{r}) V_{ext}(\vec{r}) d^3r$$

$$+ \frac{1}{2} \int \frac{n(\vec{r}) n(\vec{r}\,')}{|\vec{r} - \vec{r}\,'|} d^3r d^3r' + E_{xc}[n]$$

$$V(\vec{r}) = V_{ext}(\vec{r}) + \int d^3r' \frac{n(\vec{r}\,')}{|\vec{r} - \vec{r}\,'|} + V_{xc}[n(\vec{r})]$$

Self-interaction correction (SIC)

Perdew and Zunger, PRB23(1981)5048

$$E_G^{SIC}[n] = E_G^{LDA}[n]$$

$$-\frac{1}{2}\sum_i \int d^3r d^3r' \frac{n_i(\vec{r}) n_i(\vec{r}')}{|\vec{r}-\vec{r}'|} - \sum_i E_{xc}[n_i]$$

$$V_i^{SIC}(\vec{r}) = V^{LDA}(\vec{r}) - \int d^3r' \frac{n_i(\vec{r}')}{|\vec{r}-\vec{r}'|} - V_{xc}[n_i(\vec{r})]$$

Basic idea of LDA+U

PRB 44 (1991) 943, PRB 48 (1993) 169

- Delocalized s and p electrons : LDA
- Localized (strongly correlated) d or f electrons : +U

  using on-site d-d Coulomb interaction (Hubbard-like term)

  $U\Sigma_{i\neq j}n_i n_j$ instead of averaged Coulomb energy

  $UN(N-1)/2$

nonmagnetic
semiconductor
or insulator
C, Si

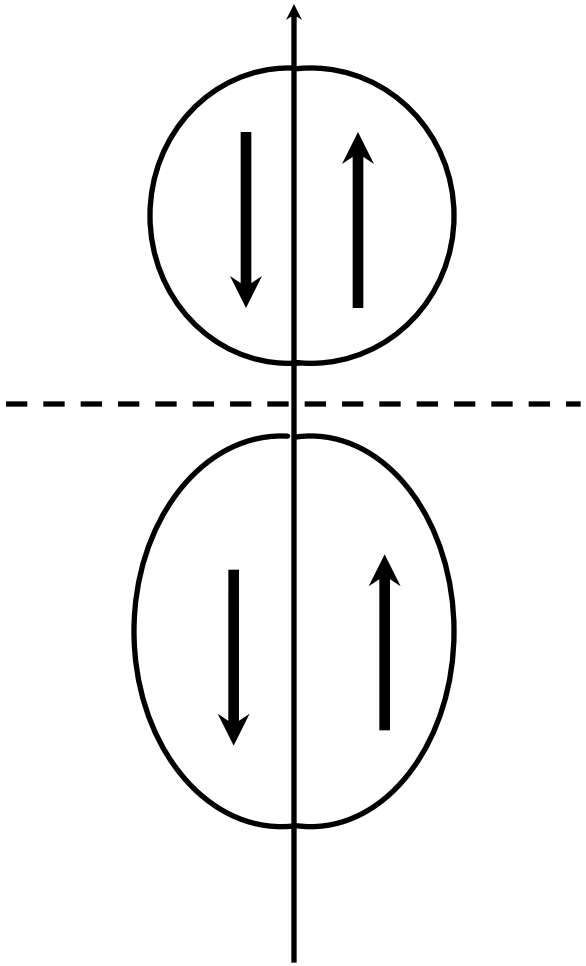

nonmagnetic
metal
Cu,Ag,Au

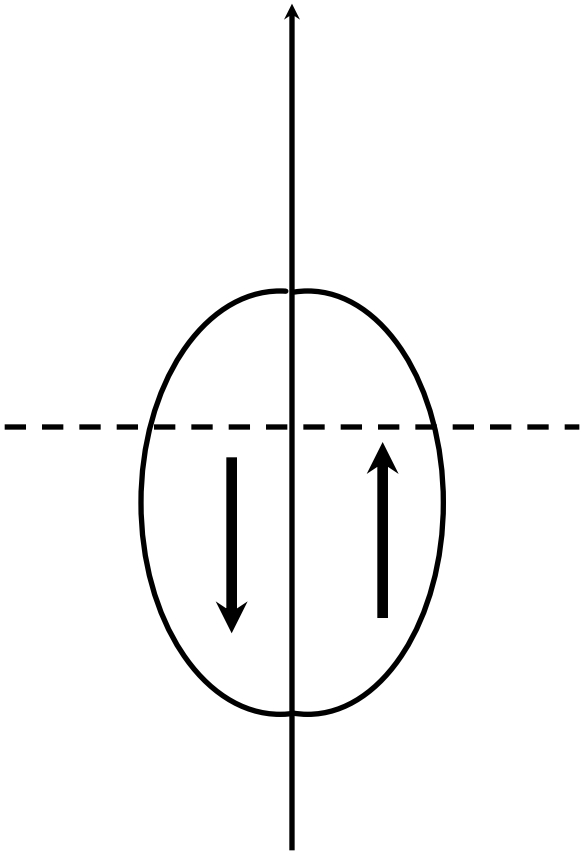

magnetic
metal
Fe,Co,Ni

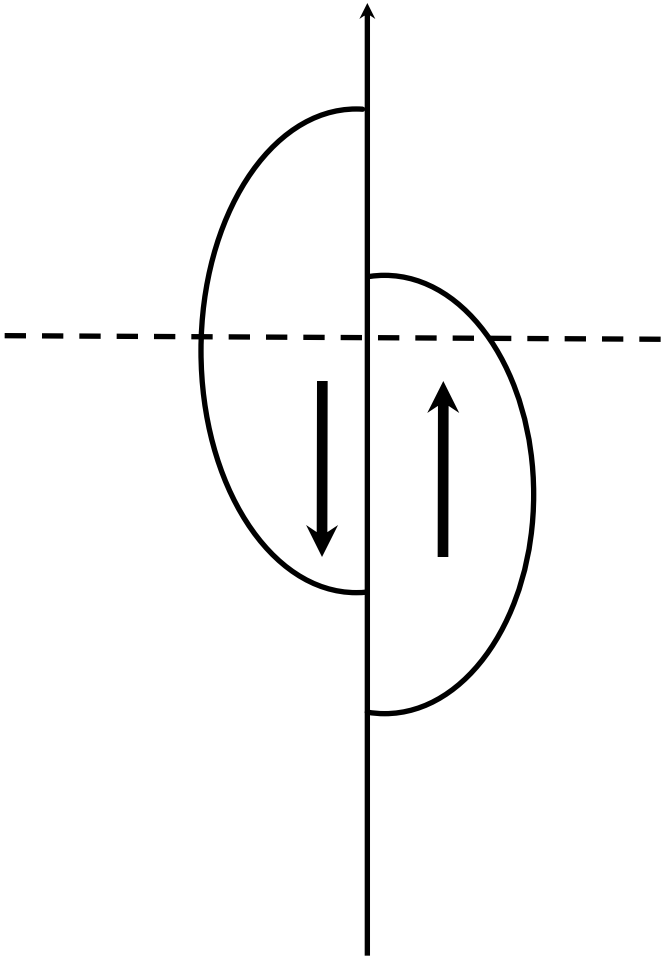

Half-metal
CrO_2, Fe_3O_4(high-T),
double perovskite
Sr_2FeMoO_6
(Spintronics)

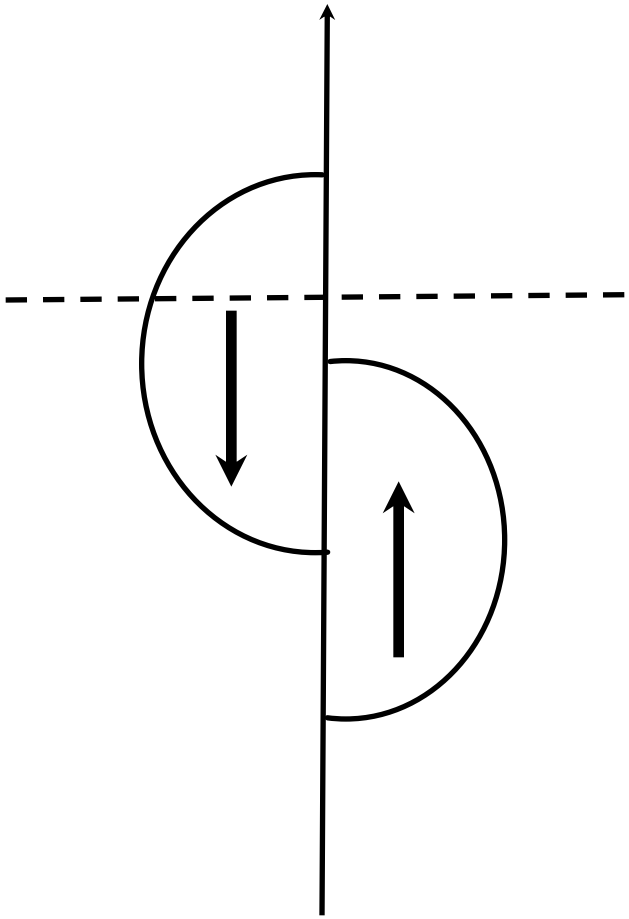

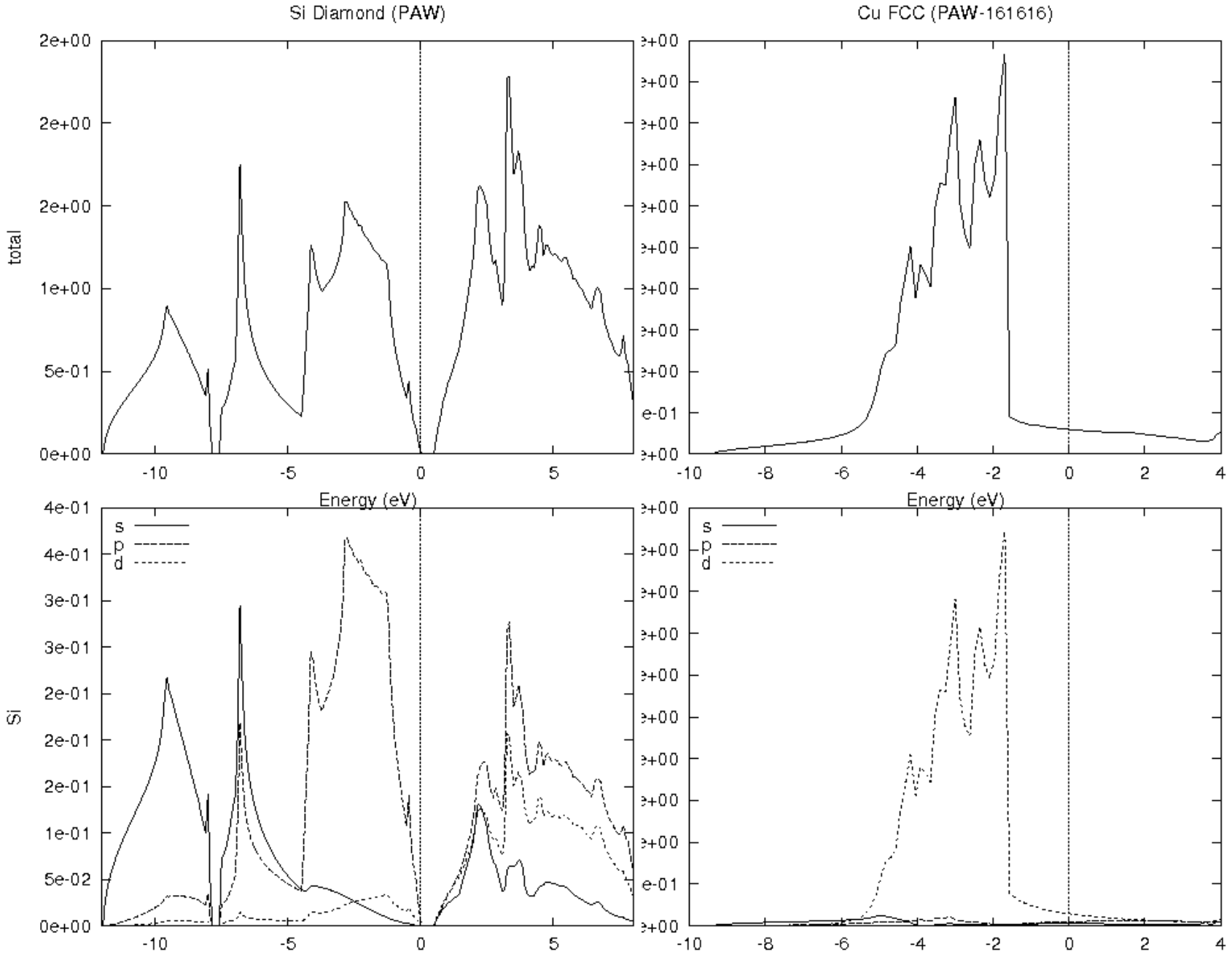
Si Diamond (PAW)
Cu FCC (PAW-161616)
total
Si
Energy (eV)
Energy (eV)
s
p
d
s
p
d
2e+00
2e+00
2e+00
1e+00
5e-01
0e+00
4e-01
4e-01
3e-01
3e-01
2e-01
2e-01
2e-01
1e-01
5e-02
0e+00
e-01
e-01
-10
-5
0
5
-10
-8
-6
-4
-2
0
2
4

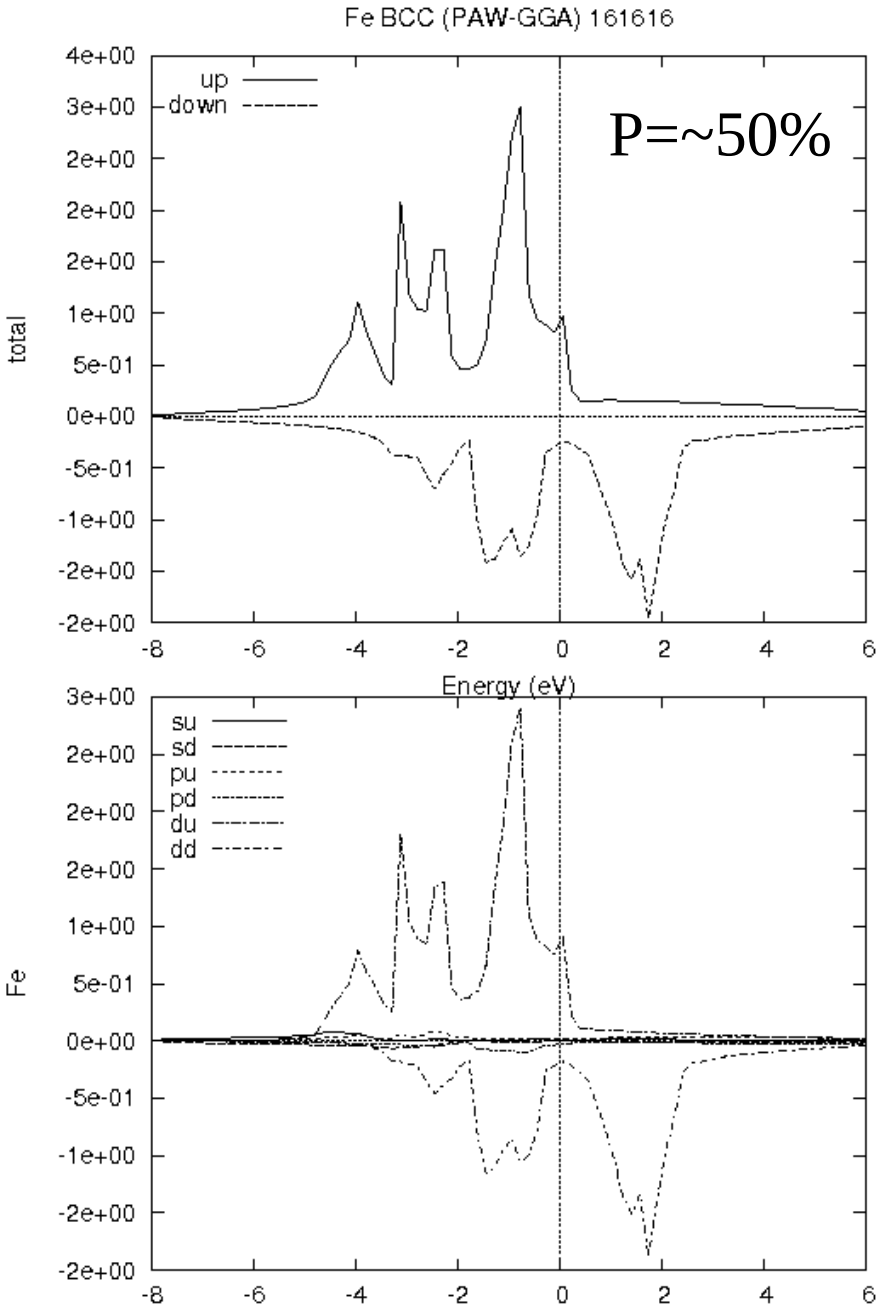

Spin polarization:
P=(n↑-n↓)/ (n↑+n↓)
around Ef

CrO2:
P(the)=100%
P(exp)=95~98%

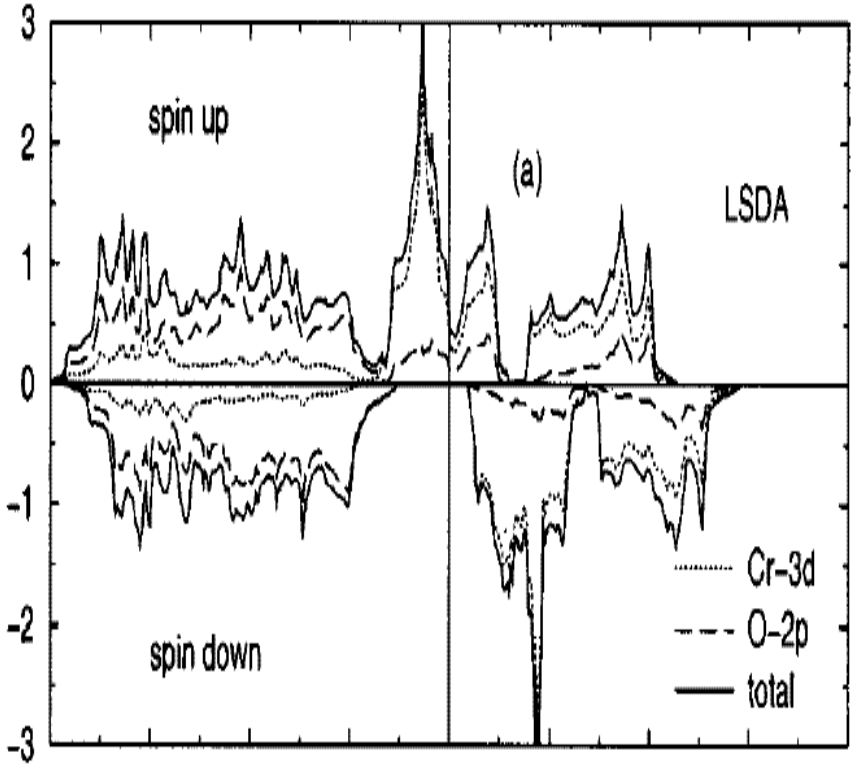

Rutile CrO2

- Half-metal, moment = $2\mu_B$
- Lattice type : bct
- 6 atoms in bct unit cell
- Space group : $P4_2/mnm$
- a = 4.419A, c=2.912A, u=0.303
- Ionic model : $Cr^{+4}(3d^2)$, $O^{-2}(2p^6)$
- U = 3.0 eV, J = 0.87 eV

Rutile structure

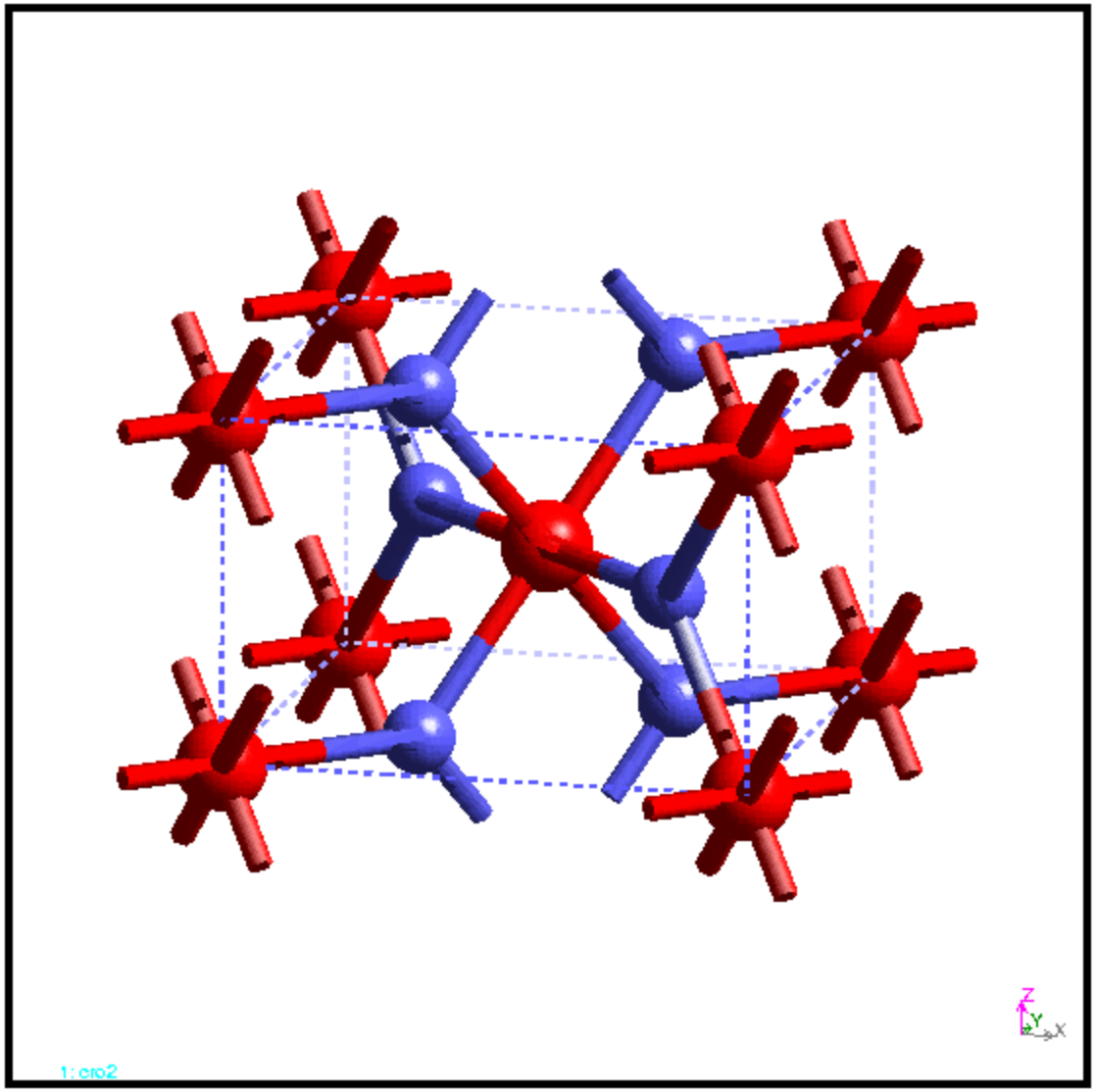

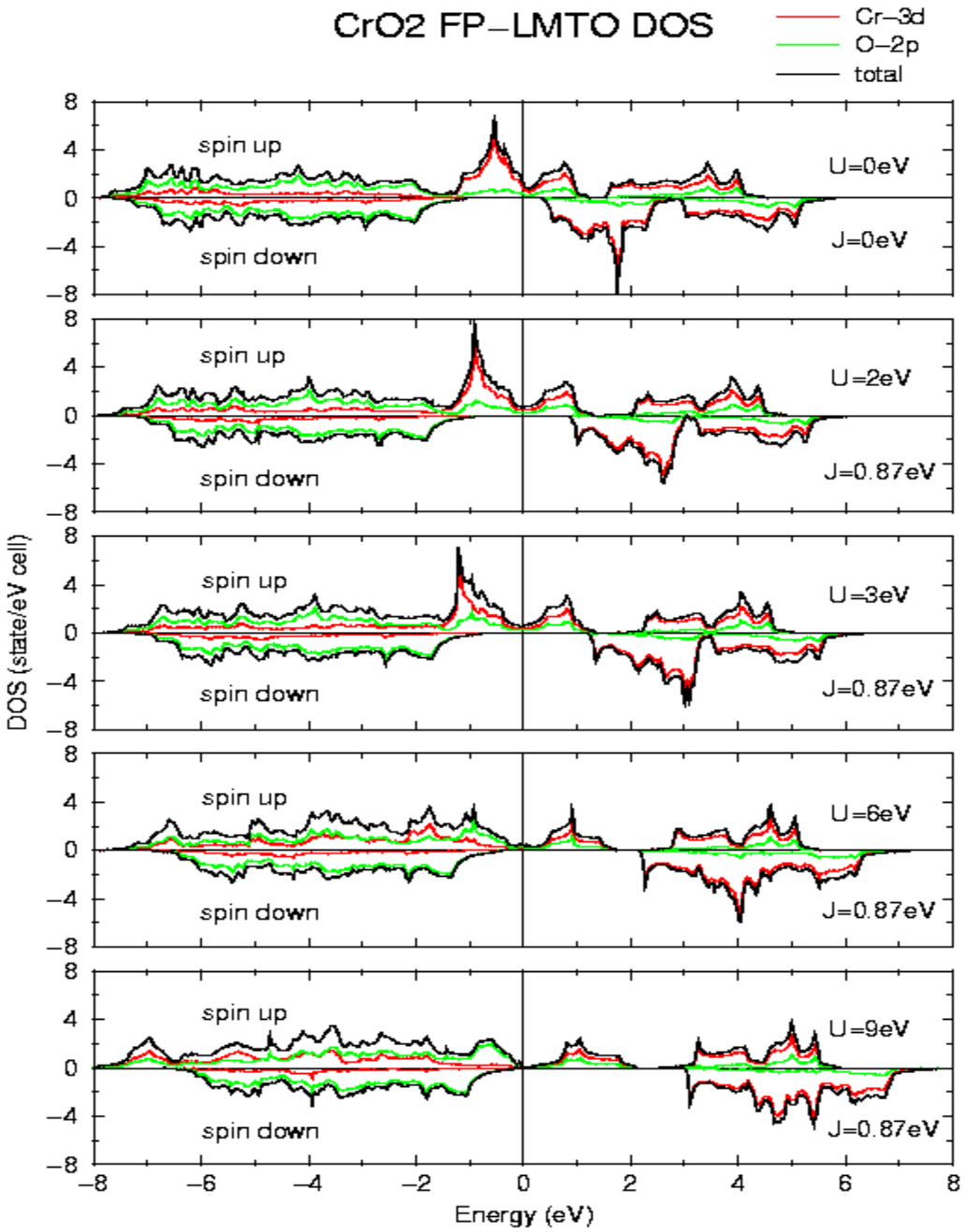
CrO2 FP−LMTO DOS
Cr−3d
O−2p
total
spin up
spin down
U=0eV
J=0eV
U=2eV
J=0.87eV
U=3eV
J=0.87eV
U=6eV
J=0.87eV
U=9eV
J=0.87eV
DOS (state/eV cell)
Energy (eV)
8
4
0
−4
−8
−8
−6
−4
−2
0
2
4
6
8

PRB 56
(1997) 15509

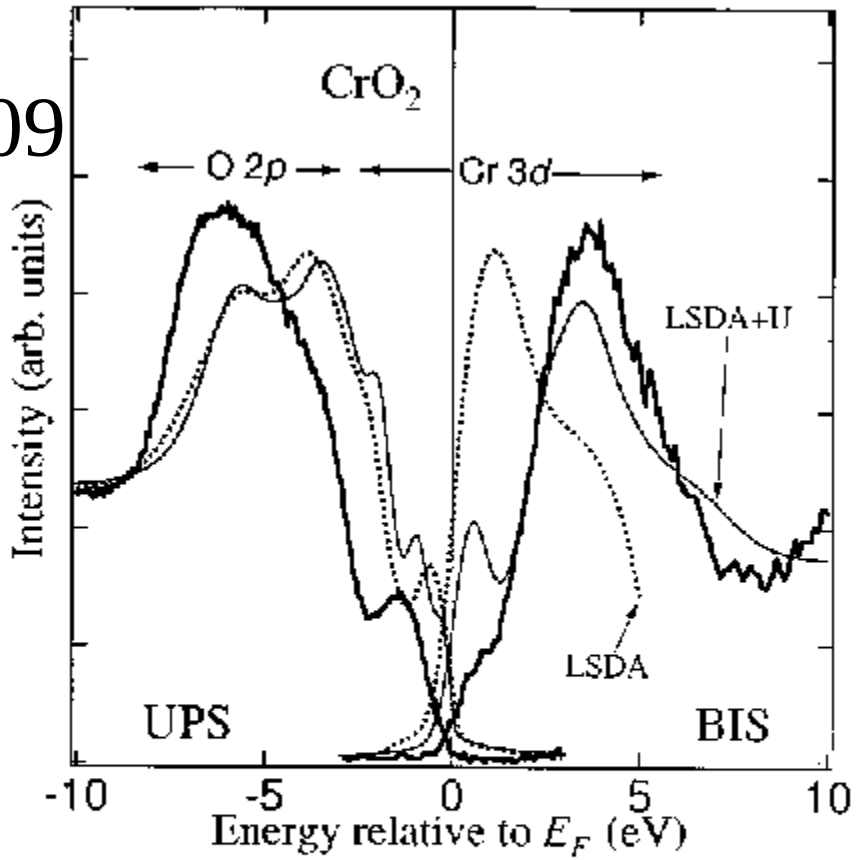

FIG. 4. UPS ($h\nu = 40.8$ eV) and BIS ($h\nu = 1486.6$ eV) spectra (solid curves) compared with theoretical spectra deduced from the LSDA (Ref. 3) and LSDA+U (Ref. 8) calculations (dashed curves).

Double perovskites :
Sr2FeMoO6, Sr2FeReO6, Sr2CrWO6

- Half-metal, moment = 4, 3, 2μ_B
- Lattice type : tet, fcc, fcc
- 40 atoms in tet, fcc, fcc unit cell
- Space group : I4/mmm, Fm3m, Fm3m
- a = 7.89, 7.832, 7.878A, c/a=1.001, 1, 1
- Ionic model : $Fe^{+3}(3d^5)$, $Cr^{+3}(3d^3)$, $Mo^{+5}(4d^1)$, $Re^{+5}(5d^2)$, $W^{+5}(5d^1)$
- U(Fe,Cr) = 4,3 eV, J(Fe,Cr) = 0.89, 0.87 eV

Double perovskite structure

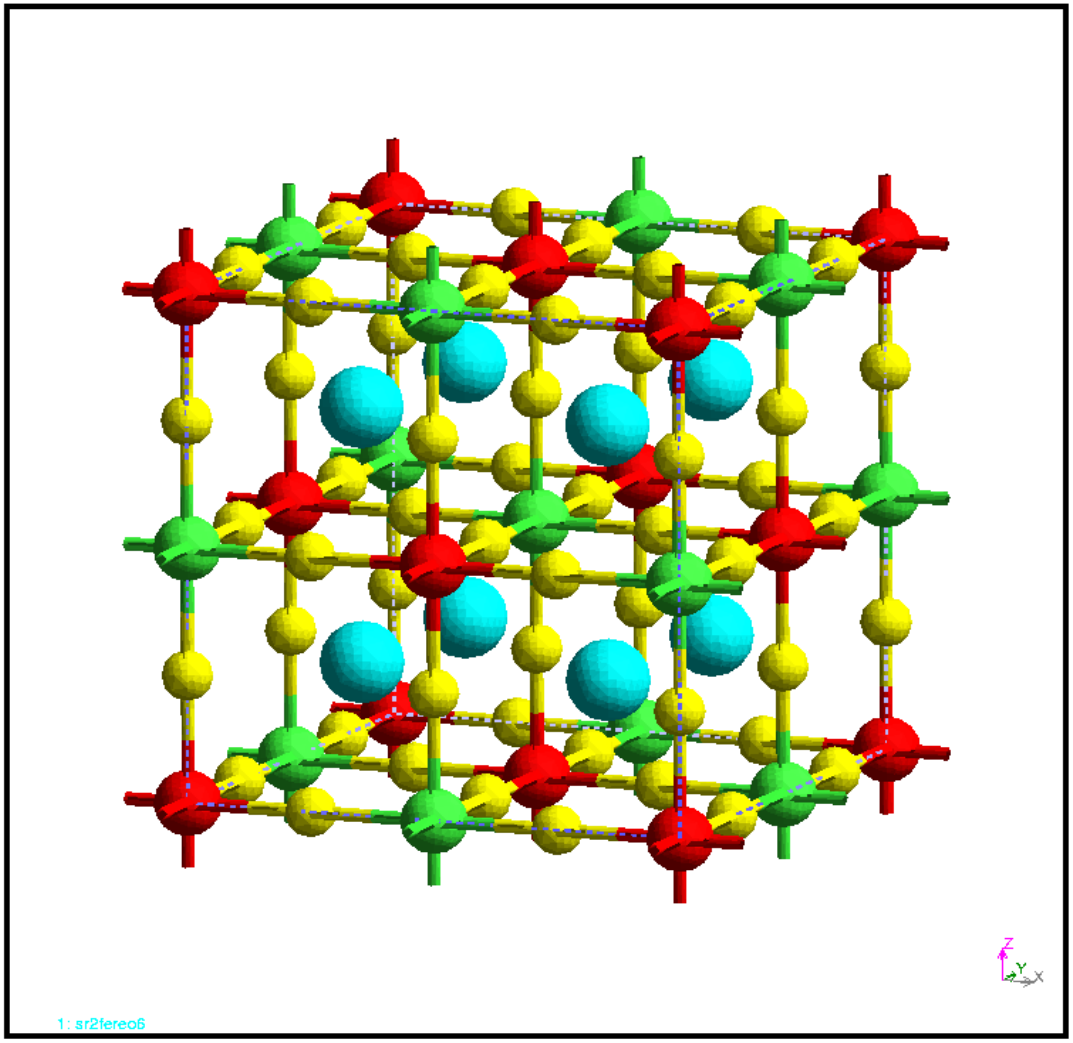

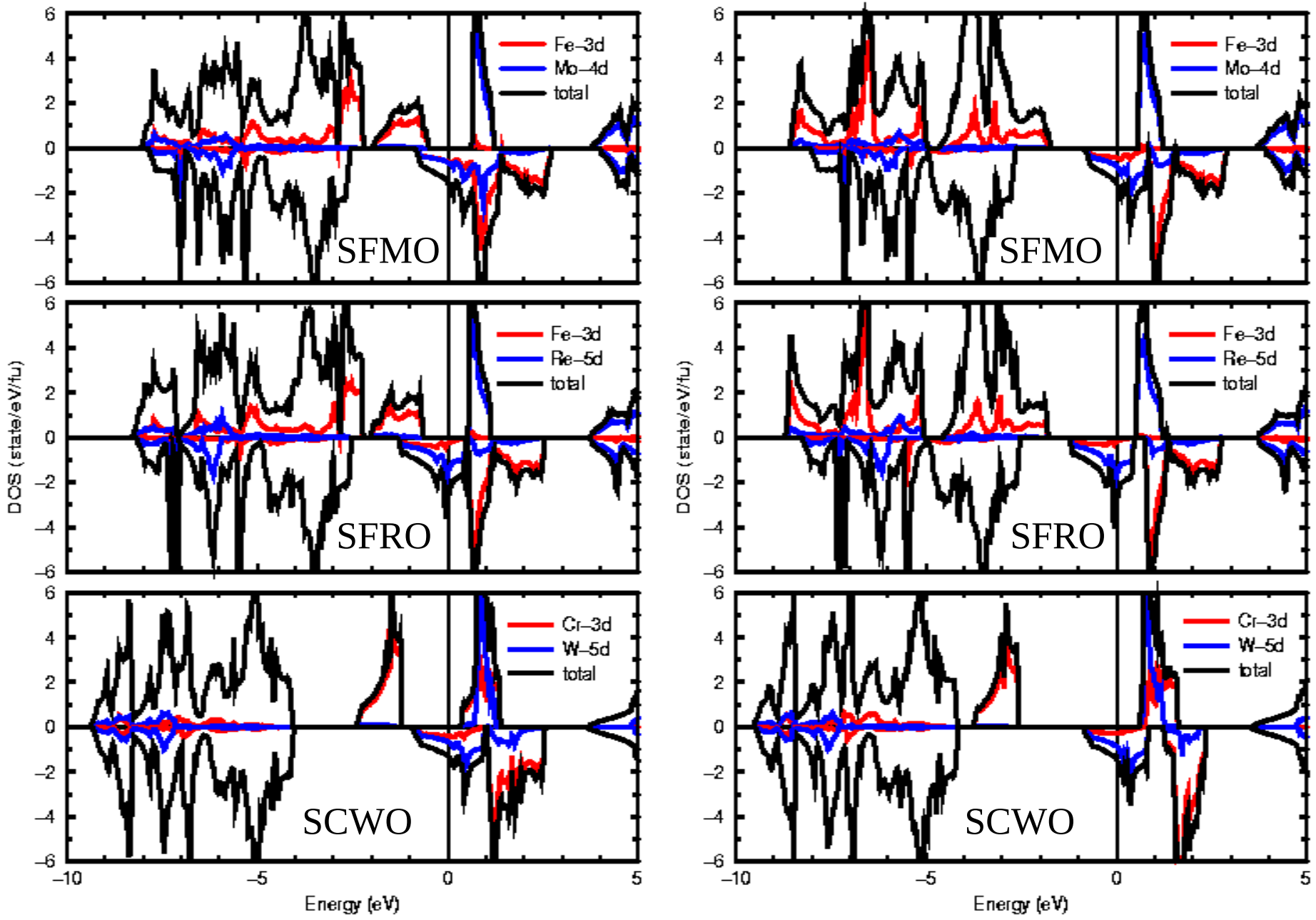
LDA
LDA+U
Fe–3d
Mo–4d
total
SFMO
Fe–3d
Re–5d
total
SFRO
Cr–3d
W–5d
total
SCWO
DOS (state/eV/fu)
Energy (eV)
6
4
2
0
–2
–4
–6
–10
–5
0
5

Magnetite (high temperature) : Fe_3O_4, $CoFe_2O_4$, $NiFe_2O_4$

- Half-metal, insulator, moment = 4, 3, $2\mu_B$
- Lattice type : fcc
- Space group : Fd3m
- 56 atoms in fcc unit cell
- a = 8.394, 8.383, 8.351 A
- Ionic model : $Fe^{+3}(3d^5)$, $Fe^{+2}(3d^6)$, $Co^{+2}(3d^7)$, $Ni^{+2}(3d^8)$
- U(Fe^{+3},Fe^{+2},Co^{+2},Ni^{+2})=4.5, 4.0, 7.8, 8.0eV
- J(Fe,Co,Ni) = 0.89, 0.92, 0.95eV

Spinel structure

Author:
Date: Sun May 21 16:31:45 2000

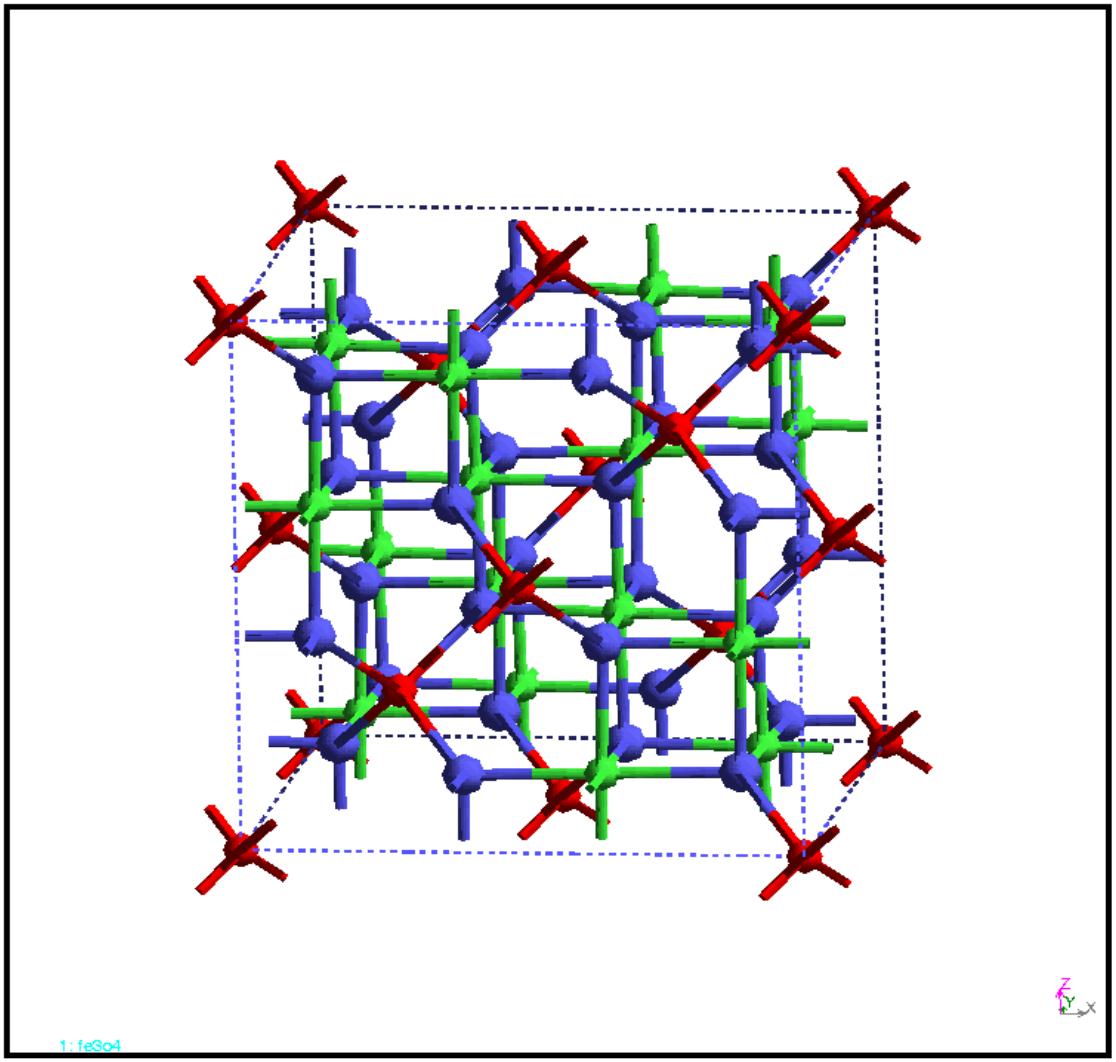

Fe_3O_4

(PES, XAS: D.J. Huang, SRRC)

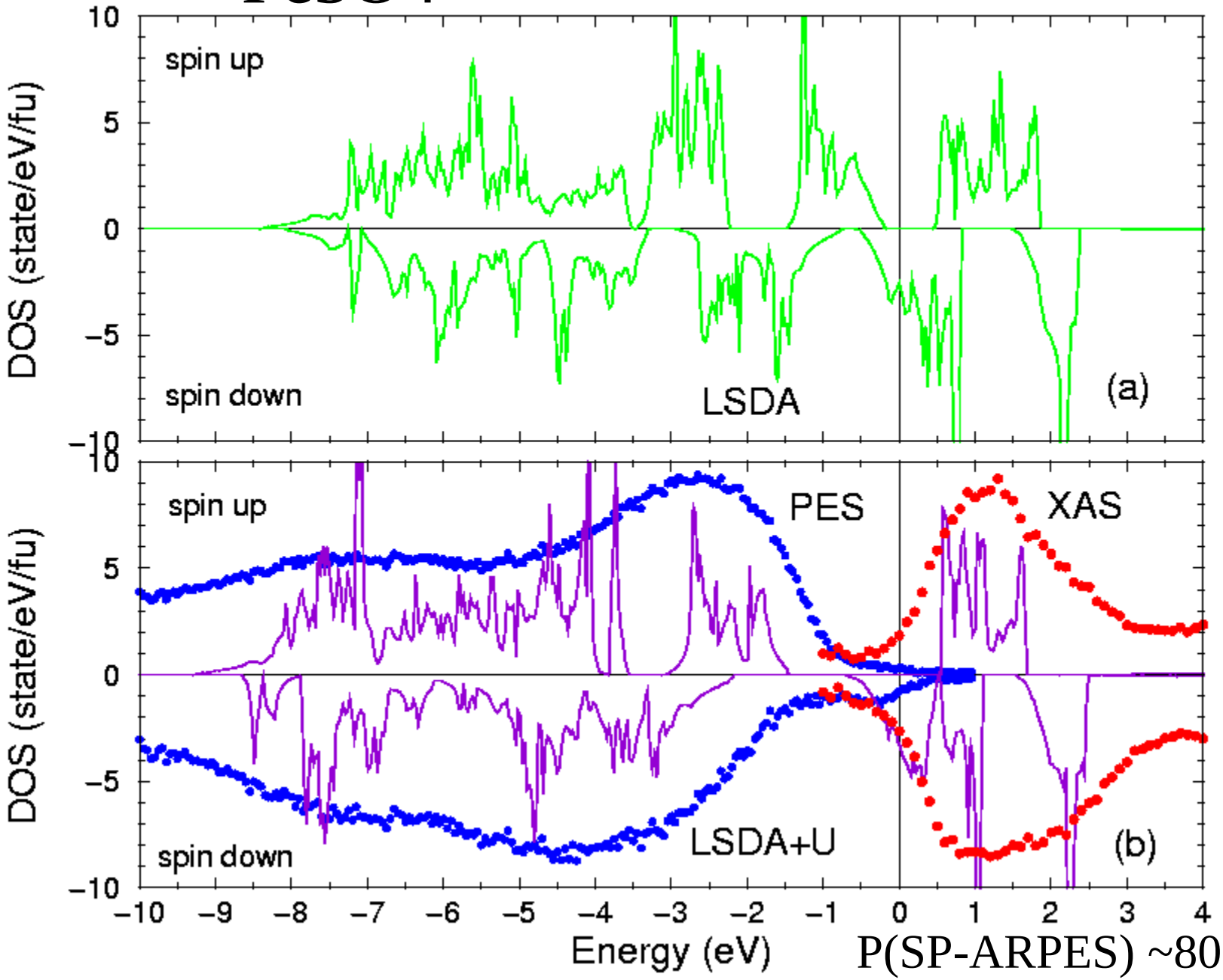

P(SP-ARPES) ~80%

Ruthenium based oxides

- Sr_2RuO_4: Nature372 (1994) 532, superconductor, Tc ~ 1 K
- Ca_2RuO_4: PRB60 (1999) R8422, AFM Mott-Hubbard insulator
- $SrRuO_3$: the only FM metal (Tc~160K) in 4d transition-metal oxides
- $CaRuO_3$: suppressed magnetic and metallic properties
- Is electron correlation important in 4d orbitals?

Transport properties, thermodynamic properties, and electronic structure of $SrRuO_3$

P. B. Allen*
Institut Romand de Recherche Numérique en Physique des Materiaux (IRRMA), IN-Ecublens, CH-1015 Lausanne, Switzerland and Departement de Physique de la Matière Condensée, Université de Genève, 24 Quai Ernest-Ansermet, CH-1211 Geneva 4, Switzerland

PRB53(1996)4393

H. Berger, O. Chauvet, and L. Forro
École Polytechnique Federale de Lausanne, Departement de Physique, CH-1015 Lausanne, Switzerland

T. Jarlborg, A. Junod, B. Revaz, and G. Santi
epartement de Physique de la Matière Condensée, Université de Genève, 24 Quai Ernest-Ansermet, CH-1211 Geneva 4, Switzerlan

(Received 22 August 1995)

$SrRuO_3$ is a metalli
coefficient for tempera
have been calculated
moment of $1.45\mu_B$ pe
the theoretical value b
resistivity increases n
resistivity saturation w
and exhibits both a lo

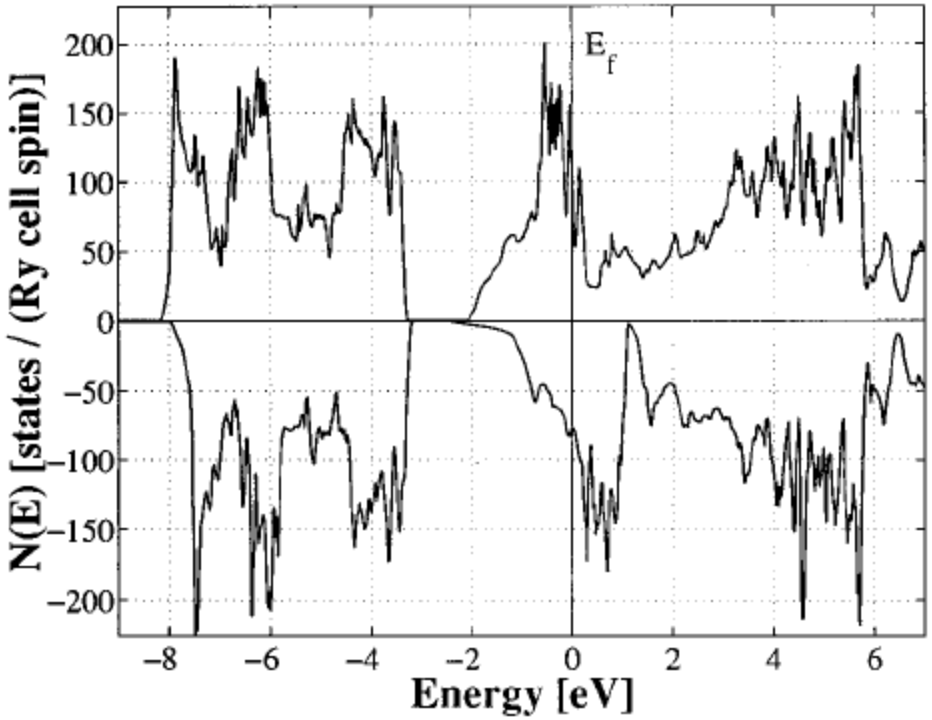

up to 1000 K, its Hall
) K. The energy bands
ferromagnetic ordered
nJ/mol, which exceeds
$f \approx 10$ Å is found. The
rt mean free path that
the Curie temperature,
perature.

$1.45\mu_B$

JAP79(1996)4818

Electronic and magnetic properties of the 4*d* itinerant ferromagnet $SrRuO_3$

David J. Singh
Complex Systems Theory Branch, Naval Research Laboratory, Washington, DC 20375

Density functional calculations are used to elucidate the electronic and magnetic structure of $SrRuO_3$. Itinerant ferromagnetic behavior is found both in the cubic perovskite and the actual orthorhombic structure. The calculated moment is 1.59 μ_B. Unusually strong hybridization is evident in both the electronic structure and magnetism. The Fermi velocities indicate significant spin differentiation of the transport properties. [S0021-8979(96)17408-6]

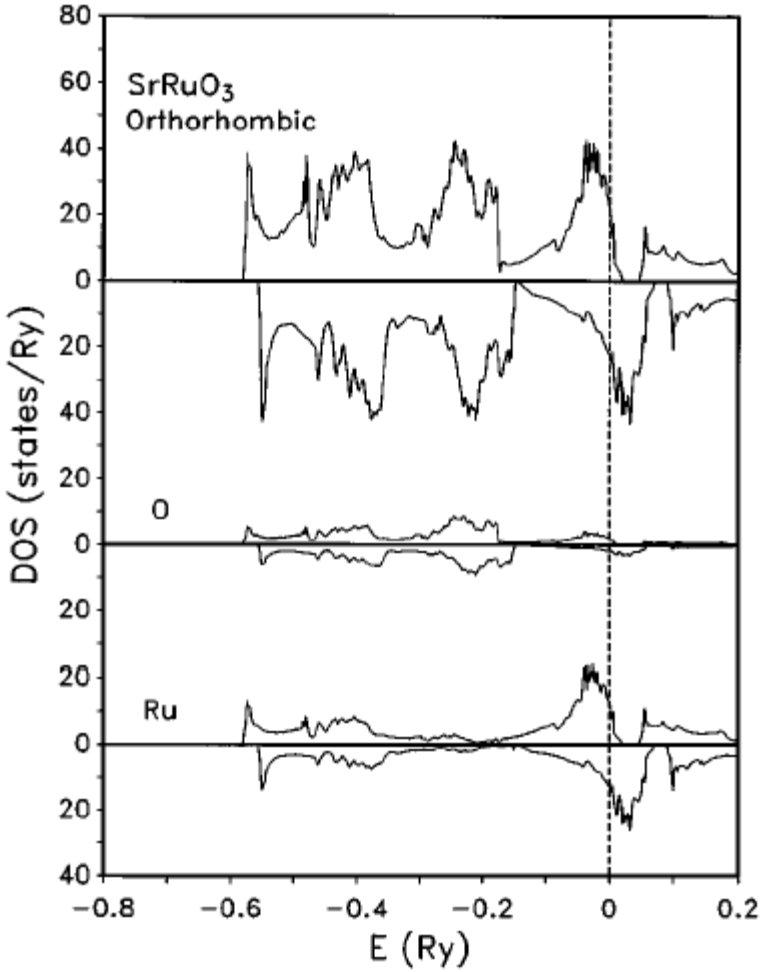

$1.59\mu_B$

PRB56(1997)2556

Electronic structure and magnetism in Ru-based perovskites

I. I. Mazin
Complex Systems Theory Branch, Naval Research Laboratory, Washington, D.C. 20375-5320
and CSI, George Mason University, Fairfax, Virginia 22030

D. J. Singh
Complex Systems Theory Branch, Naval Research Laboratory, Washington, D.C. 20375-5320
(Received 19 February 1997)

The magnetic properties of ruthenates with perovskite-derived structures, particularly (Ca,Sr)RuO_3 and Sr_2YRuO_6, are studied within the context of band-structure-based Stoner theory. First principles calculations are used to demonstrate that in all cases the correct magnetic behavior and order can be obtained without recourse to strong correlation effects and that the insulating character of Sr_2YRuO_6 is reproduced. The different magnetic states of $SrRuO_3$ and $CaRuO_3$ are shown to be due to the different structural distortions in these materials, most significantly the larger rotation of the octahedra in the Ca compound. $CaRuO_3$ is found to be on the verge of a ferromagnetic instability, leading to the expectation of giant local moments around magnetic impurities and other anomalous effects in analogy with fcc Pd metal. Oxygen $2p$-derived states hybridize strongly with Ru d states in all three compounds, and O, through this hybridization, plays an unusually large role in the magnetic properties. This involvement of O is responsible for the strong magnetostructural coupling that is found in the calculations. Transport properties of $CaRuO_3$ and $SrRuO_3$ are analyzed using the calculated Fermiology. Unusually large magnon and paramagnon couplings are found, which are consistent with reported measurements of the low-temperature specific heat and the resistivity coefficient. [S0163-1829(97)05829-3]

Thermal, magnetic, and transport properties of single-crystal $Sr_{1-x}Ca_xRuO_3$ ($0 \leqslant x \leqslant 1.0$)

G. Cao, S. McCall, M. Shepard, and J. E. Crow
National High Magnetic Field Laboratory, Florida State University, Tallahassee, Florida 32310

PRB56(1997)321

R. P. Guertin*
Physics Department, Tufts University, Medford, Massachusetts 02155

(Received 24 January 1997)

$SrRuO_3$ is a highly correlated, narrow d-band metal which undergoes a ferromagnetic transition at $T_c = 165$ K. $CaRuO_3$, which is also a highly correlated metal, has the same crystal structure, comparable electrical resistivity and similar effective Ru moment, but it remains paramagnetic at least down to 1 K. High- and low-field magnetization and susceptibility, thermoremanent magnetization, low-temperature heat capacity, electrical resistivity, and Hall effect measurements are presented on as-grown, untwinned, orthorhombic single-crystal samples of $Sr_{1-x}Ca_xRuO_3$ for the entire concentration range $0 \leqslant x \leqslant 1.0$. T_c is depressed uniformly with increasing x, all the way to $x = 1.0$, with possible spin-glass-type ordering for x close to 1.0. The critical Sr doping of paramagnetic $CaRuO_3$ required to cause magnetic correlations among the Ru moments is $\cong 1$ at.%. Magnetization to 7 T shows strong hysteresis for mixed ($x > 0$) crystals only, with evidence for a rotation of the easy magnetic axis out of the ab plane. Low-temperature magnetization in dc fields to 30 T for $x = 0$ shows a lack of saturation to the full $S = 1$ moment, $2\mu_B$/Ru atom, underscoring the itinerant character of the ferromagnetism. Similar data for $x = 1.0$ show it to be a highly exchange enhanced paramagnet, a borderline antiferromagnet or ferromagnet. This is consistent with previous Ru-O in-plane and out-of-plane doping studies. Low-temperature heat capacity ($1 < T < 20$ K) shows that the mass enhancement ($\gamma = 29$ mJ/mol K^2 and $m^* \approx 3$ for $x = 0$) and the Debye temperature ($\Theta_D = 390$ K for $x = 0$) are nonmonotonically varying with increasing x. The large electrical resistivity suggests these materials are ''bad'' metals, with a mean free path at room temperature ≈ 10 A for $x = 0$. The Hall effect shows a sign reversal for $x = 0$ and $x = 1.0$, but not for mixed crystals. The data are compared where it is appropriate to data derived from comparable experiments from polycrystalline samples and from epitaxially grown thin films. The results support the highly electron-correlated nature of ordered magnetism in Ru-based oxides and the results should help to advance our understanding of the transport, magnetic, and thermodynamic properties of bad metals.

PRB56(1997)6380

Electronic structure of $SrRuO_3$

LSDA~-0.5eV

K. Fujioka, J. Okamoto, T. Mizokawa, and A. Fujimori*
Department of Physics, University of Tokyo, Bunkyo-ku, Tokyo 113, Japan

I. Hase
Electrotechnical Laboratory, Umezono, Tsukuba

M. Abbate
Laboratorio Nacional de Luz Sincrotron, Campinas, Caixa Postal 619

H. J. Lin and C. T. Chen
Synchrotron Radiation Research Center, Hsinchu 30077, Tai

Y. Takeda
Department of Chemistry, Faculty of Engineering, Mie Uni

M. Takano
Institute for Chemical Research, Kyoto University, Uji, Kyoto 611, Japan

(Received 25 February 1997)

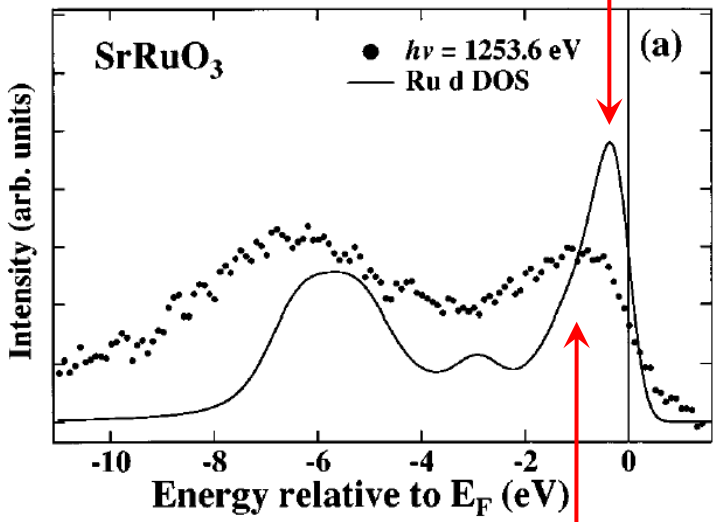

Expt.~-1.1eV

We have measured photoemission and oxygen 1*s* x-ray absorption spectra of the ferromagnetic metal $SrRuO_3$ and compared them with a first-principles band-structure calculation. The overall distribution of Ru 4*d* and O 2*p* spectral weight is in good agreement with that predicted by the band-structure calculation. However, the observed spectral line shape of the Ru 4*d* band is spread over a wide energy range and the emission intensity at the Fermi level is weakened compared to the band-structure calculation. This implies the importance of electron correlation in the Ru oxide. [S0163-1829(97)05736-6]

$SrRuO_3$

- Lattice type : orthorhombic perovskite
- Space group : Pnma (No. 62)
- 20 atoms in orthorhombic unit cell
- a=5.5332 A, b=5.57169 A, c=7.8491 A
- Ionic model : $Ru^{4+}(4d^4, t2g^3\uparrow, t2g^1\downarrow)$
- U = 3.5 eV, J = 0.58 eV
- Pseudopotential, 100 k-point, 31360 plane wave, Cut-off energy = 400 eV

Orthorhombic perovskite $SrRuO_3$

Sr

Ru

O

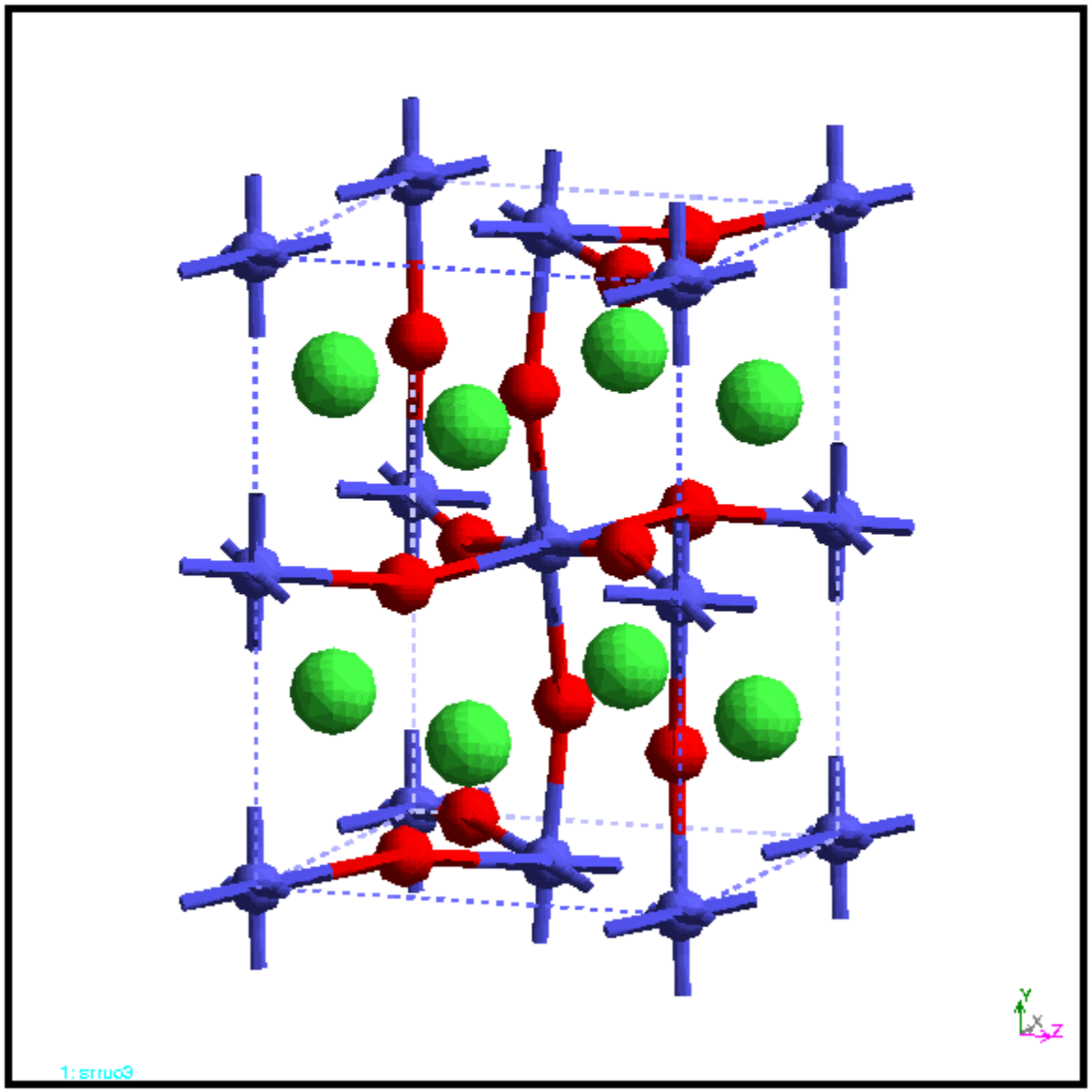

Ionic model :

$Sr^{2+}Ru^{4+}O^{2-}{}_3$: Ferromagnetic : $2\mu_B$

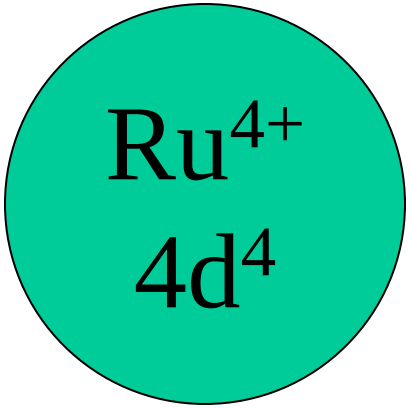

4d-t2g

↑ ↑ ↑

↓

half-metal

fully occupied, insulator
partially occupied, conductor

$SrRuO_3$

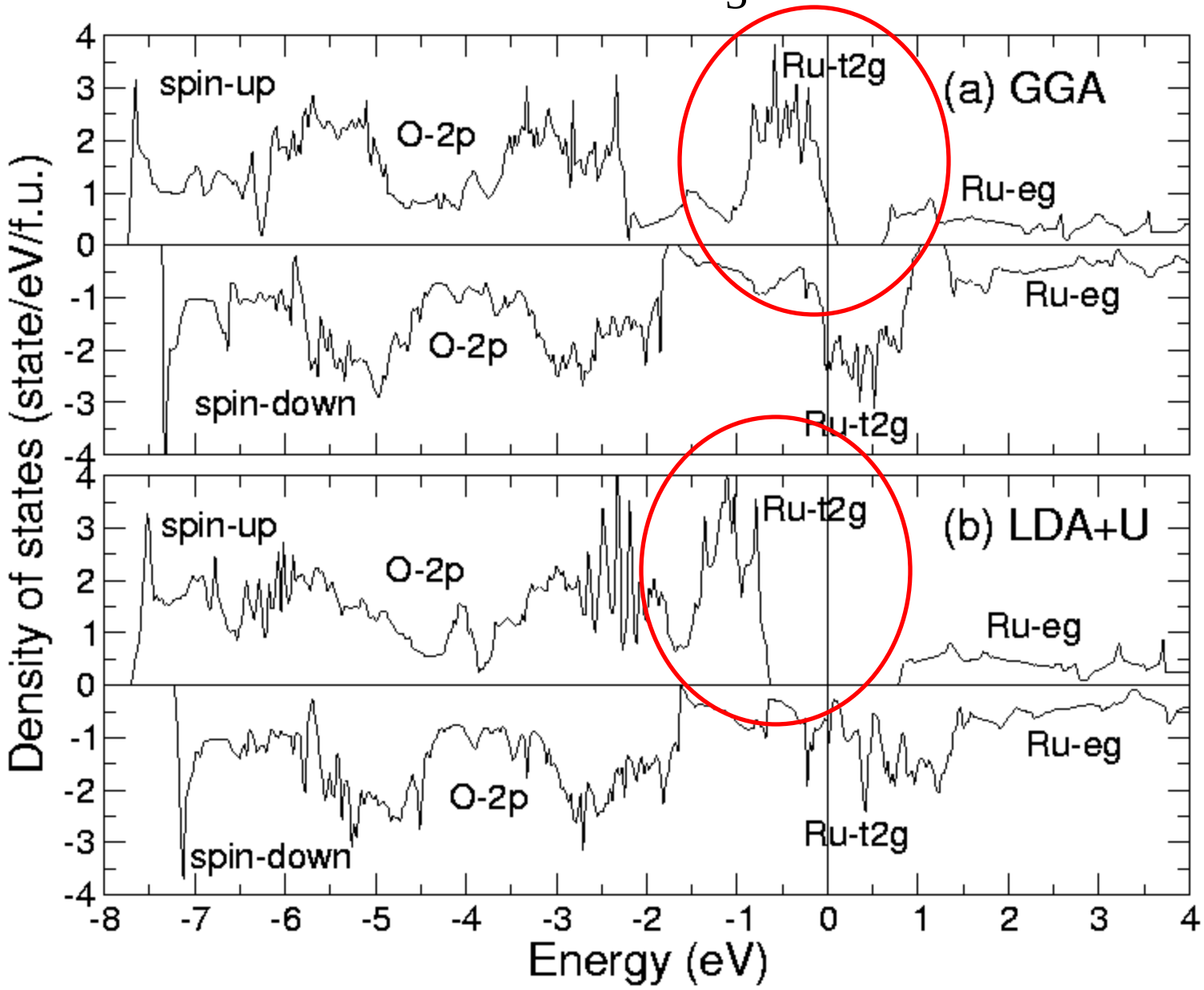

Metal

Half-metal

Orthorhombic perovskite $SrRuO_3$

Sr

Ru

O

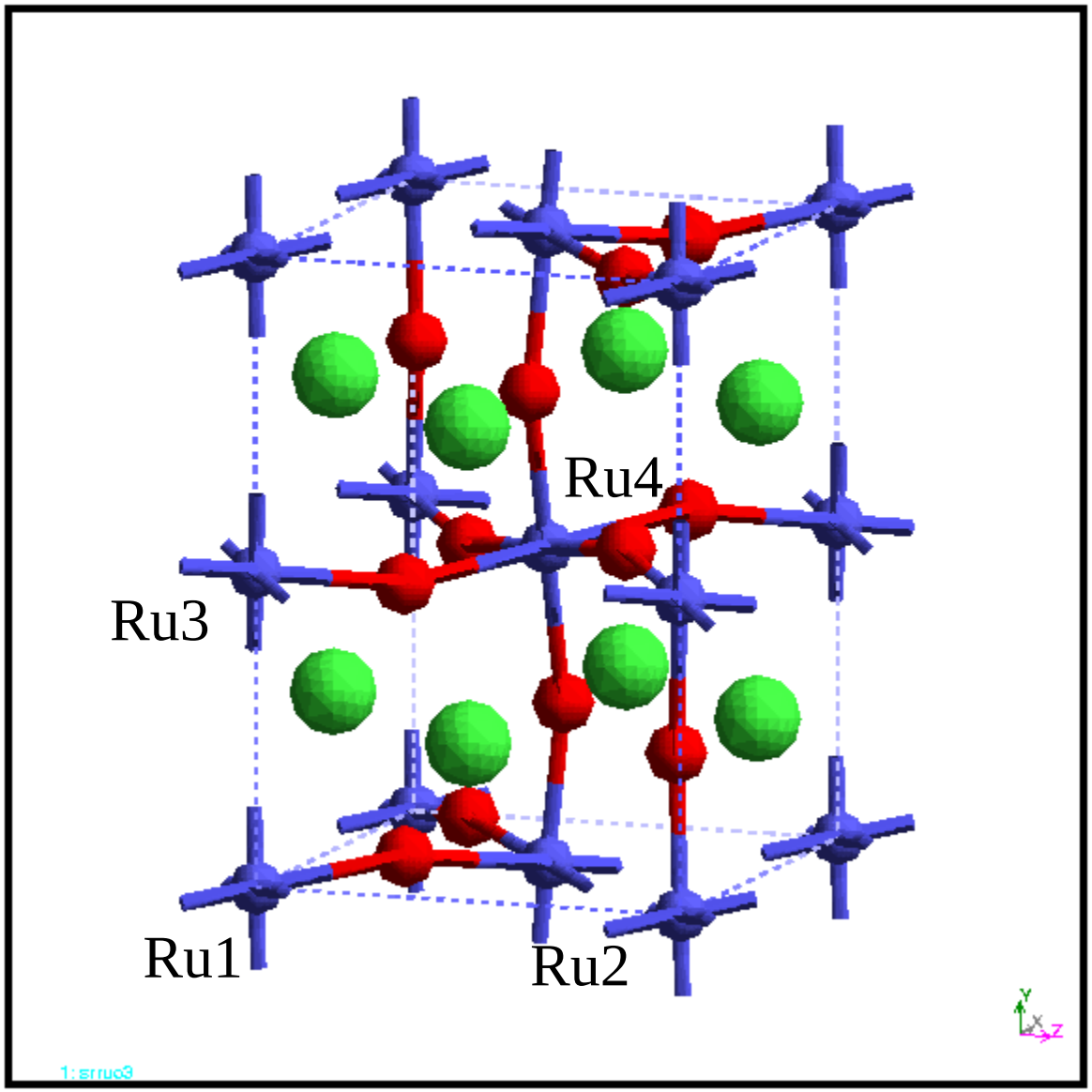

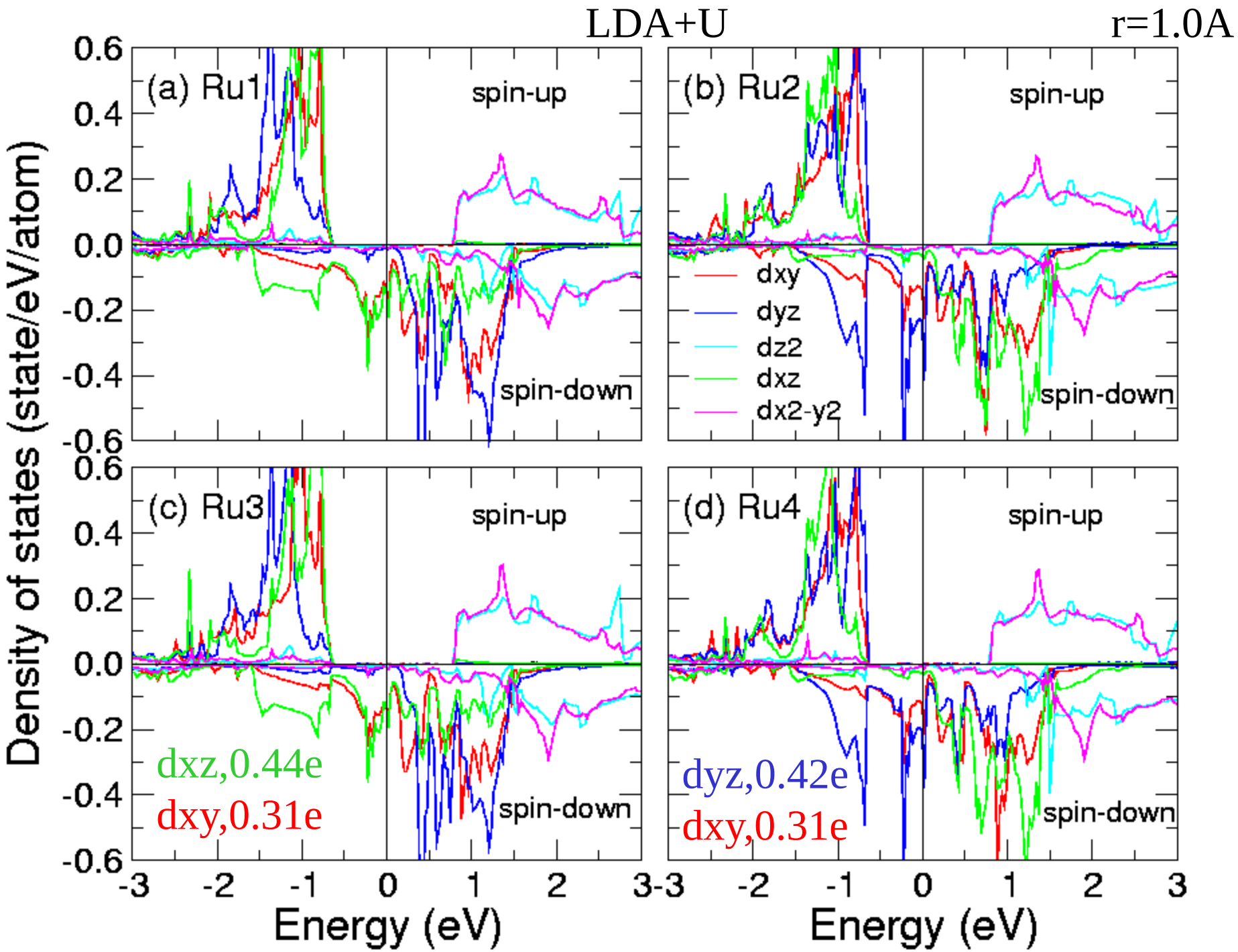
LDA+U
r=1.0A
(a) Ru1
spin-up
spin-down
(b) Ru2
spin-up
spin-down
dxy
dyz
dz2
dxz
dx2-y2
(c) Ru3
spin-up
spin-down
dxz,0.44e
dxy,0.31e
(d) Ru4
spin-up
spin-down
dyz,0.42e
dxy,0.31e
Density of states (state/eV/atom)
Energy (eV)
Energy (eV)
0.6
0.4
0.2
0.0
-0.2
-0.4
-0.6
-3
-2
-1
0
1
2
3

SrRuO3

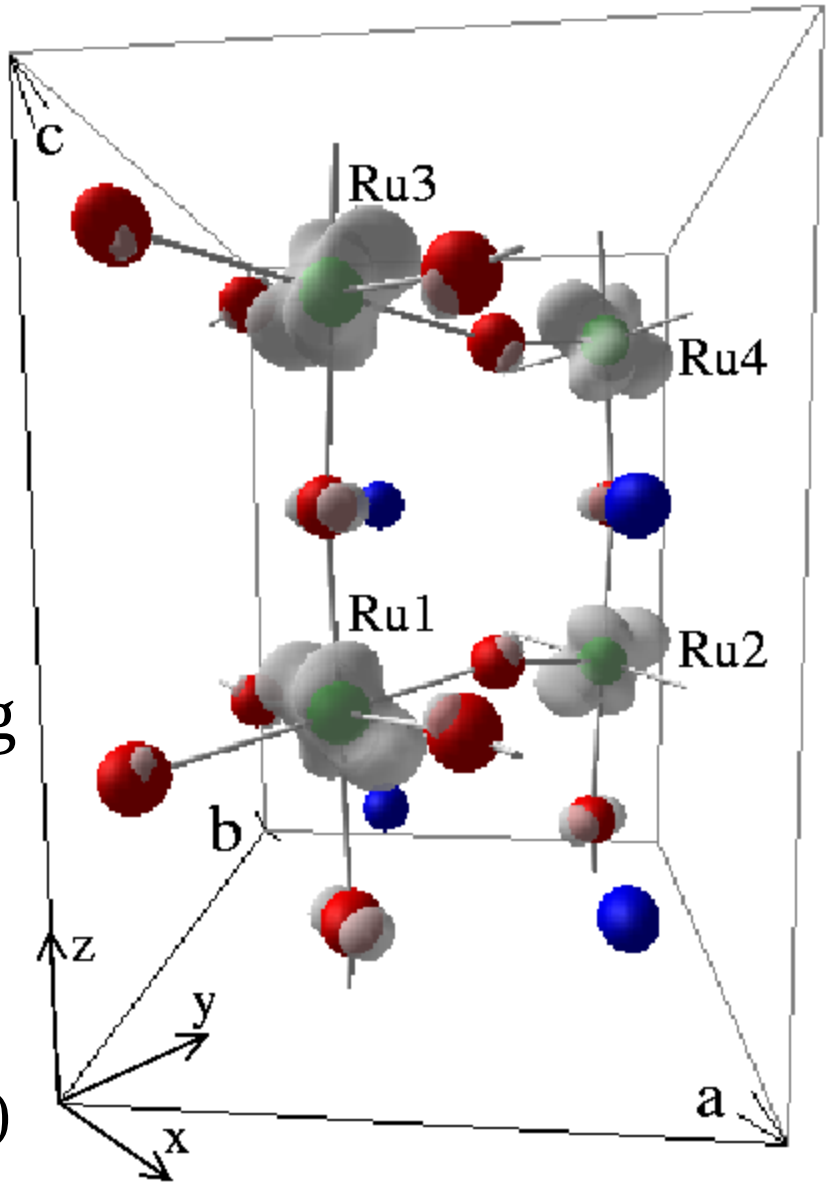

orbital ordering

(-1/3,-1/3,-1/3)

H. T. Jeng,
S. H. Lin,
C. S. Hsue
PRL97(2006)
67002

Prediction on spin polarized 2D electron gas in SrRuO3 layer in STO/SRO/STO hetrostructure

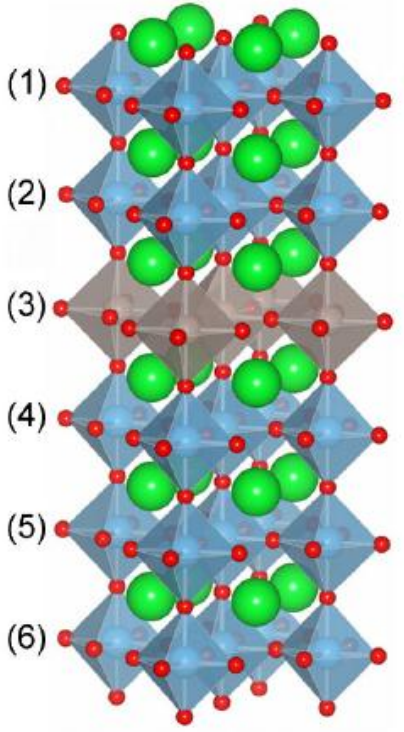

(a)

PRL 108, 107003 (2012) PHYSICAL REVIEW LETTERS

Highly Confined Spin-Polarized Two-Dimensional Electron Gas in $SrTiO_3/SrRuO_3$ Superlattices

Marcos Verissimo-Alves,[1] Pablo García-Fernández,[1] Daniel I. Bilc,[2,3] Philippe Ghosez,[2]

[1]*Departamento de Ciencias de la Tierra y Física de la Materia Condensada, Universidad de Cantabria, Cantabria Campus Internacional, Avenida de los Castros s/n, 39005 Santander, Spain*
[2]*Physique Théorique des Matériaux, Université de Liège, Allée du 6 de Août 17 (B5), B-4000 Sart Tilman, Belgium*
[3]*Molecular and Biomolecular Physics Department, National Institute for Research and Development of Isotopic and Molecular Technologies, RO-400293 Cluj-Napoca, Romania*

(Received 5 August 2011; published 8 March 2012)

We report first-principles characterization of the structural and electronic properties of $(SrTiO_3)_5/(SrRuO_3)_1$ superlattices. We show that the system exhibits a spin-polarized two-dimensional electron gas, extremely confined to the $4d$ orbitals of Ru in the $SrRuO_3$ layer. Every interface in the superlattice behaves as a minority-spin half-metal ferromagnet, with a magnetic moment of $\mu = 2.0\mu_B/SrRuO_3$ unit. The shape of the electronic density of states, half-metallicity, and magnetism are explained in terms of a simplified tight-binding model, considering only the t_{2g} orbitals plus (i) the bidimensionality of the system and (ii) strong electron correlations.

DOI: 10.1103/PhysRevLett.108.107003 PACS numbers: 74.70.Pq, 73.20.At, 75.10.−b, 75.70.−i

Multiferroic material

- A material exhibits (anti-)ferromagnetism and ferroelectricity and/or ferroelasticity simultaneously under certain temperature.
- TbMnO3 is the first ferroelectromagnet discovered in recent years.
- TbMnO3, YMnO3, HoMnO3, …
- TbMn2O5, YMn2O5, HoMn2O5, …
- Ni3V2O8, MnWO4, CoCr2O4, Ca3CoMnO6, …

Pierre Curie (1894): magnetoelectric effect: multiferroic: magnetism and ferroelectricity coexist in one compound

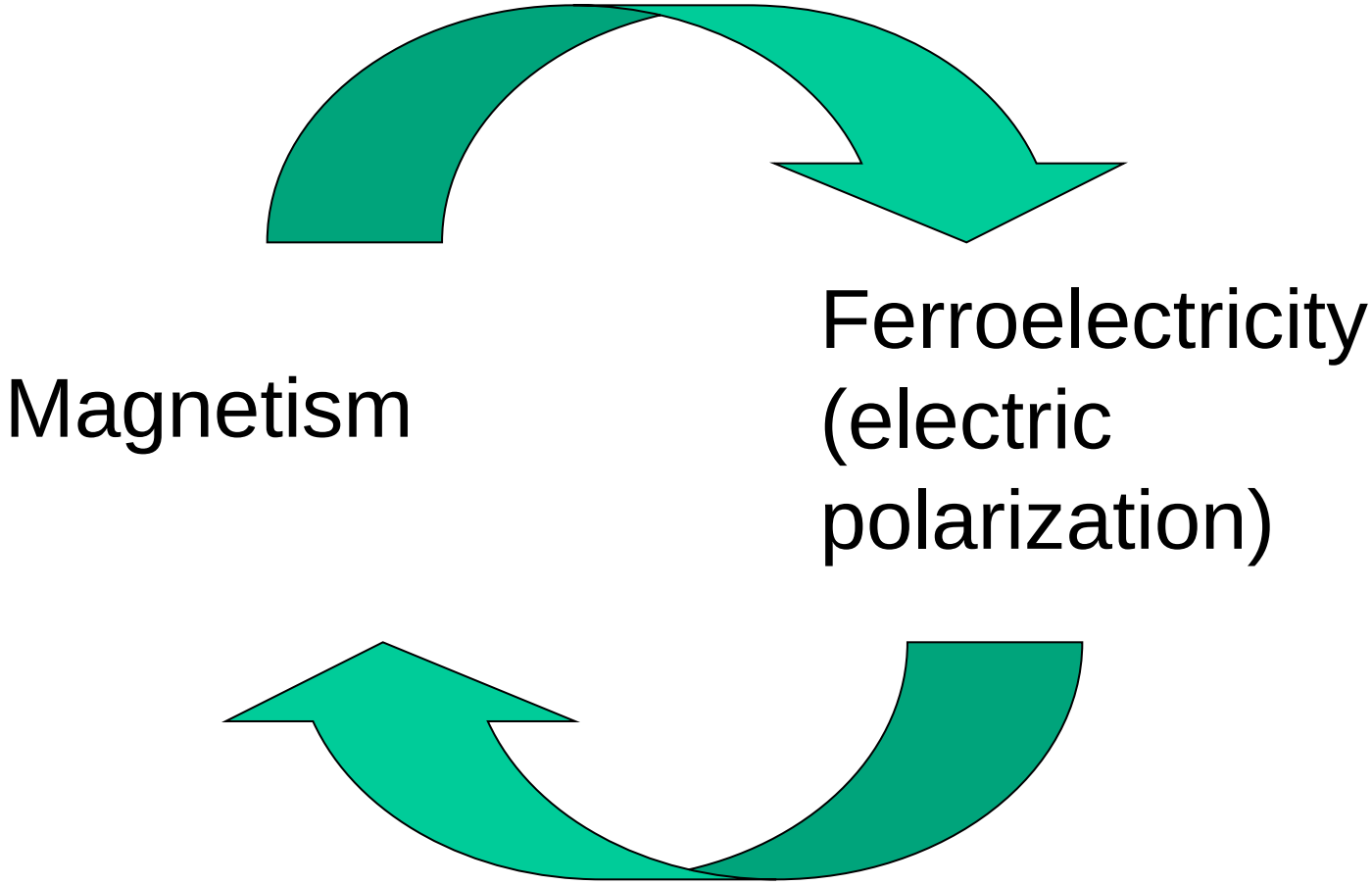

usually small, no real application, no much attention before 2003

TbMnO3
perovskite

Kimura, et al., Nature 426 (2003) 55

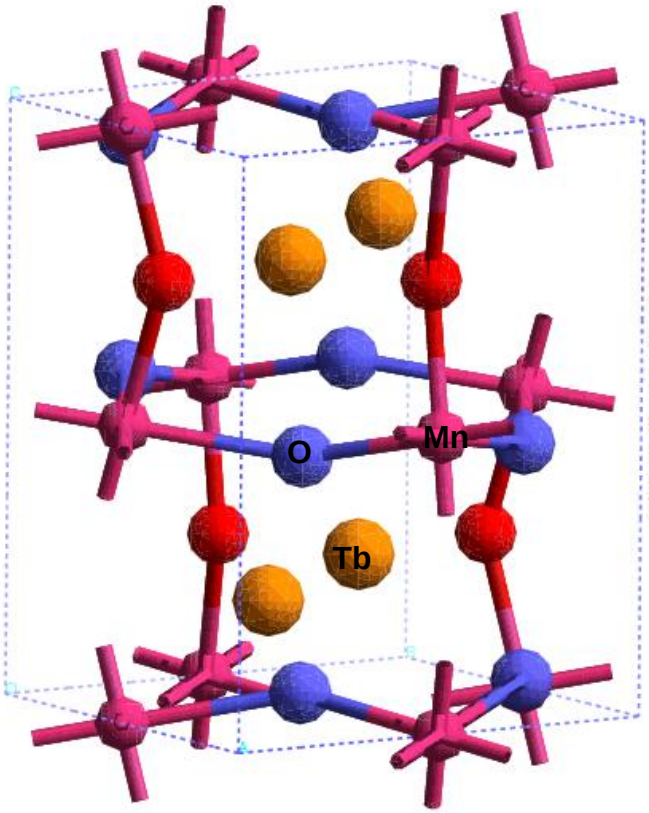

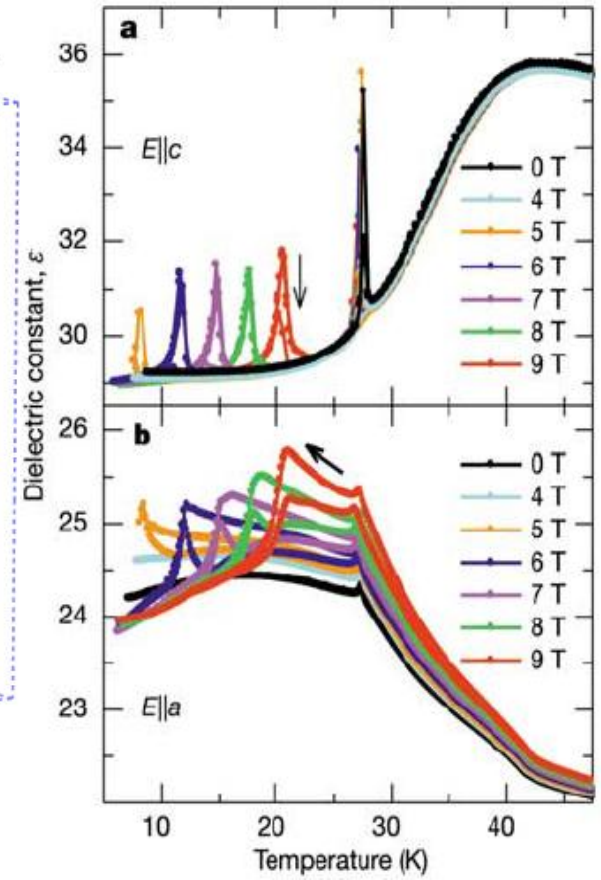

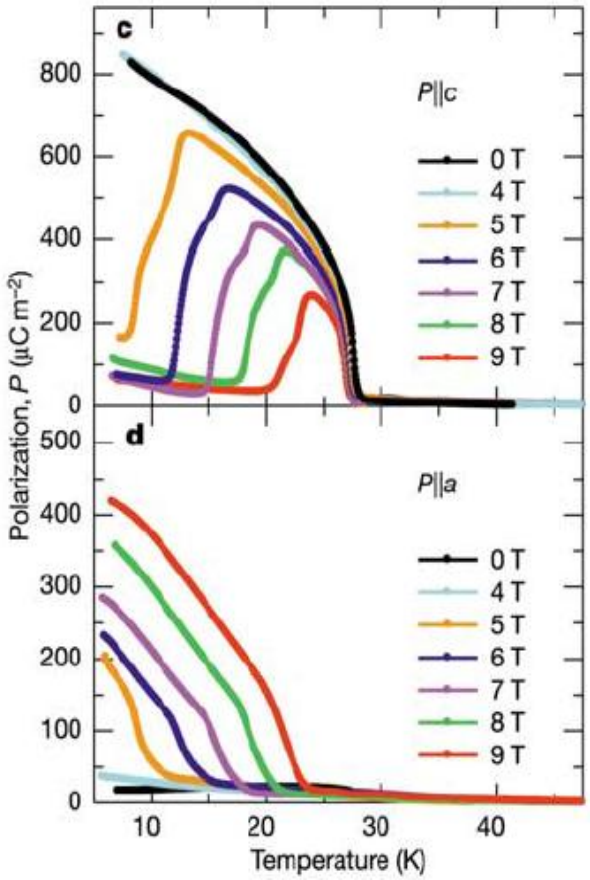

Types of multiferroic materials

- Type I: ferroelectricity and magnetism have different origins and occur at different temperatures (Fe_3O_4, $PrCaMnO_3$, $LuFe_2O_4$, …), known for a long time
- Type II: ferroelectricity is due to or related to magnetism (Ca_3CoMnO_6, $RNiO_3$, $RMnO_3$, RMn_2O_5, …), currently hot

Origin of multiferroism

- Ferroelectricity: induced by spatial inversion symmetry breaking
- Multiferroism: magnetism induced spatial inversion symmetry breaking → ferroelectricity
- Noncolinear magnetism, spiral spin arrangement, relativistic spin-orbit interaction ($YMnO_3$, …).
- Charge ordering+magnetostriction (no spin-orbit interaction) ($TbMn_2O_5$, …)

Ferroelectricity: induced by spatial inversion symmetry breaking

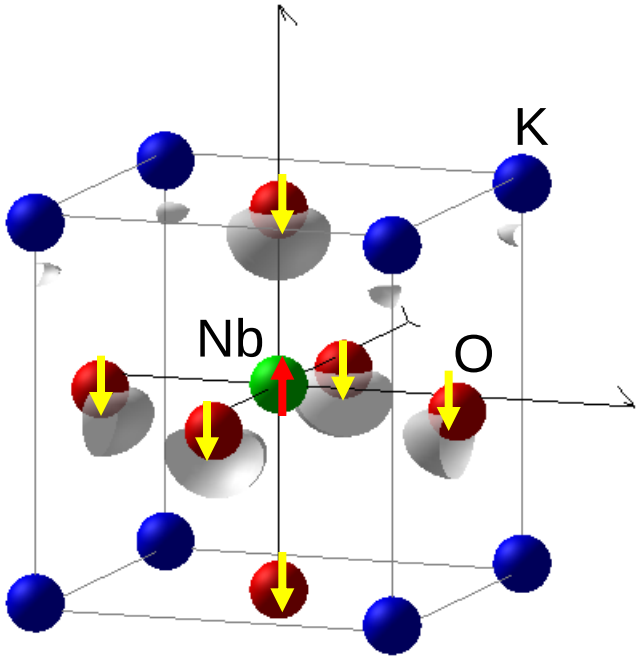

Ferroelectric perovskite KNbO3

$$\vec{P} = \vec{P}_{ion} + \vec{P}_{ele}$$

$$\vec{P}_{ion} = \sum_{n} q_i \Delta \vec{r}_i$$

$$\vec{P}_{ele} = \int \vec{r} \Delta\rho(\vec{r}) d\vec{r}$$

Multiferroism: magnetism induced spatial inversion symmetry breaking → ferroelectricity

Multiferroism: Charge ordering+magnetostriction → structural distortion → inversion symmetry breaking → electrical polarization

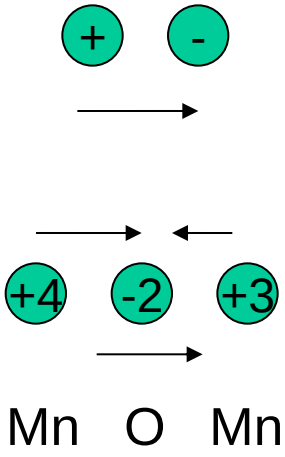

Magnetostriction → (exchangestriction, intersite exchange)

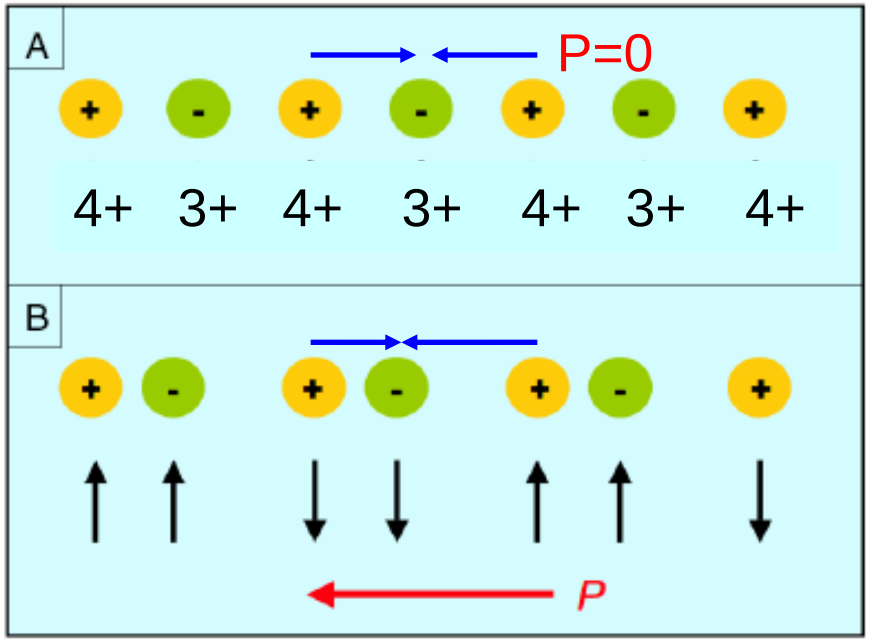

*Spontaneous (structural distortion, magnetostriction) polarization

*External (electronic, magnetic) field induced polarization

Ferroelectricity Induced by Acentric Spin-Density Waves in YMn_2O_5

L. C. Chapon,[1] P. G. Radaelli,[1,2] G. R. Blake,[1,3] S. Park,[4] and S.-W. Cheong[4]

[1]*ISIS Facility, Rutherford Appleton Laboratory-CCLRC, Chilton, Didcot, Oxfordshire, OX11 0QX, United Kingdom*

[2]*Department of Physics and Astronomy, University College London, Gower Street, London WC1E 6BT, United Kingdom*

[3]*Materials Science Division, Argonne National Laboratory, Argonne, Illinois 60439, USA*

[4]*Department of Physics and Astronomy, Rutgers University, Piscataway, New Jersey 08854, USA*

(Received 7 November 2005; published 7 March 2006)

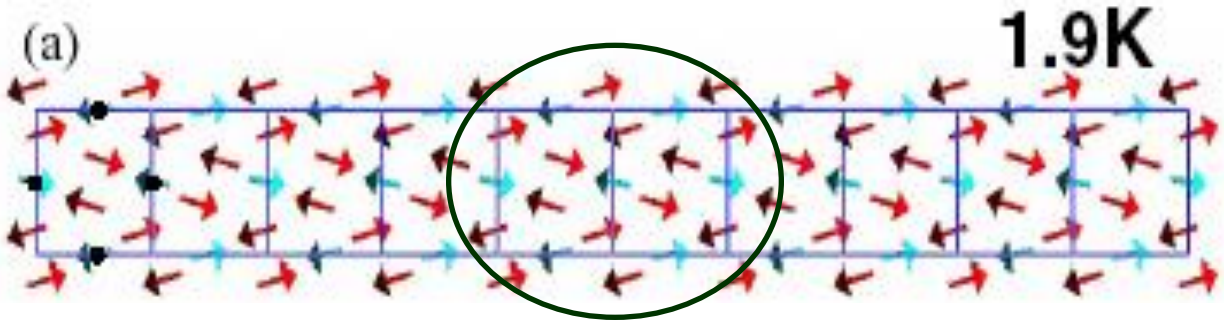

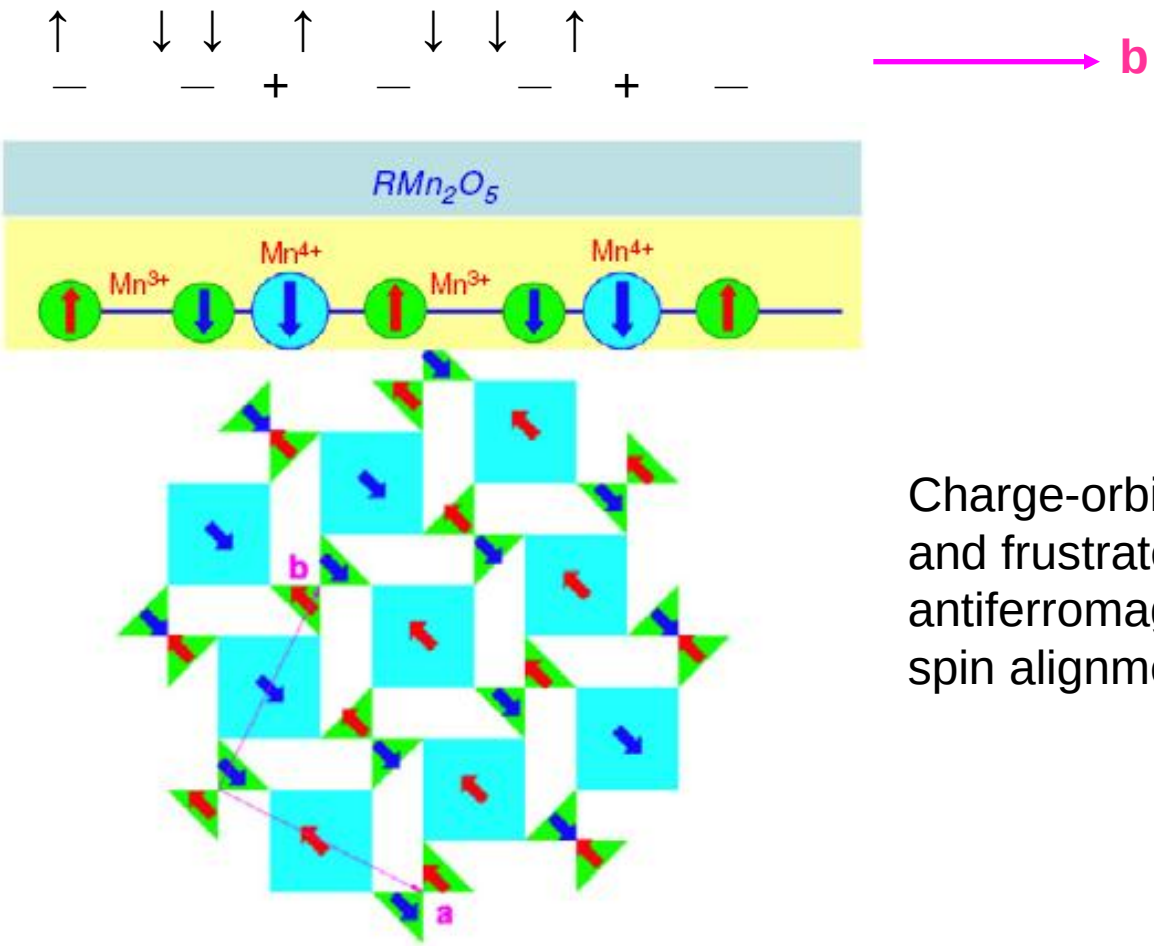

Charge-orbital ordering and frustrated antiferromagnetic spin alignment

Figure 9. Schematic view of the crystal structure of RMn_2O_5 consisting of connected $Mn^{4+}O_6$ octahedra (blue squares) and $Mn^{3+}O_5$ pyramids (green triangles); the figure is from the review of Sushkov *et al* in this issue. The chain of Mn^{3+}–Mn^{3+}–Mn^{4+} along the *b*-direction, with corresponding spin ordering, is shown in the upper panel.

Multiferroic TbMn2O5
PHYSICAL REVIEW B
84, 024421 (2011)

Origin of dz2 orbital ordering:
structural, crystal field

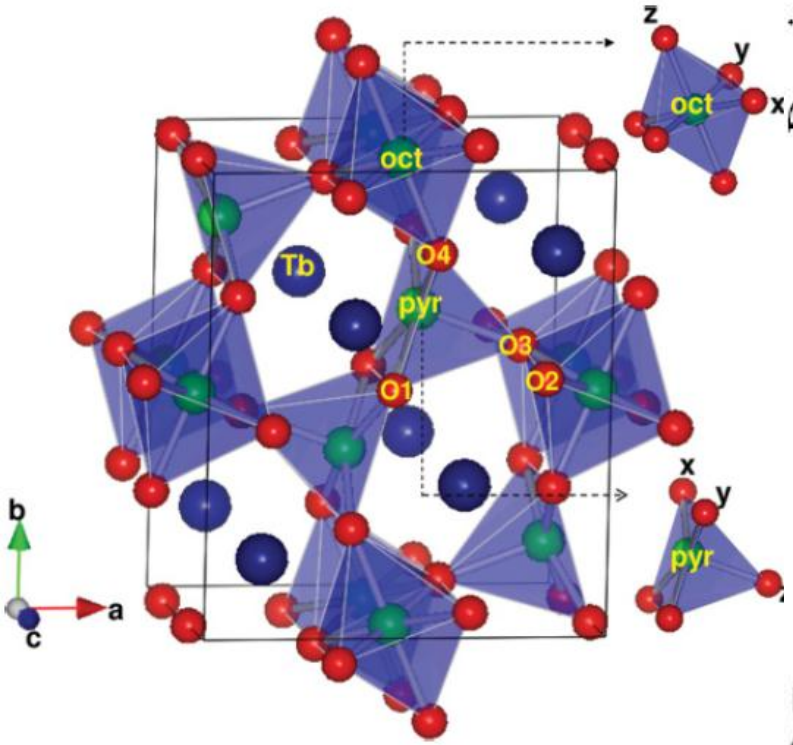

FIG. 1. (Color) Crystal structure of $TbMn_2O_5$. Blue, green, and red spheres denote Tb, Mn, and O(1–4) atoms, respectively. *abc* and *xyz* are, respectively, the crystal and local coordinates.

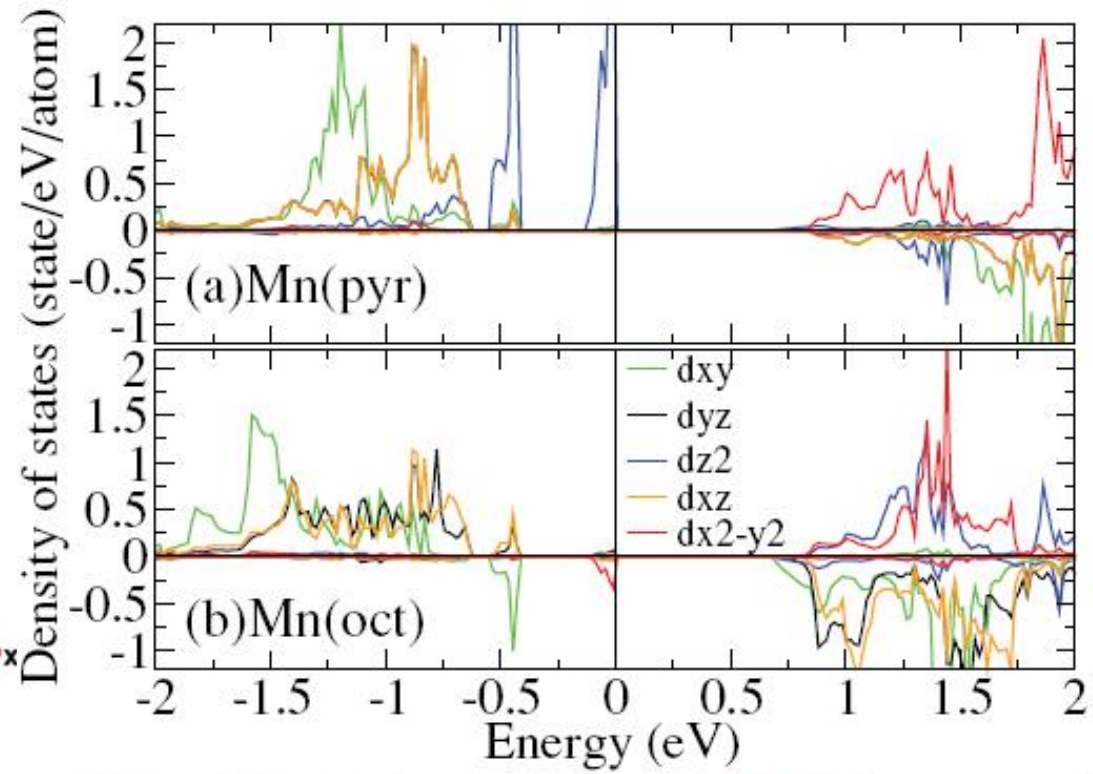

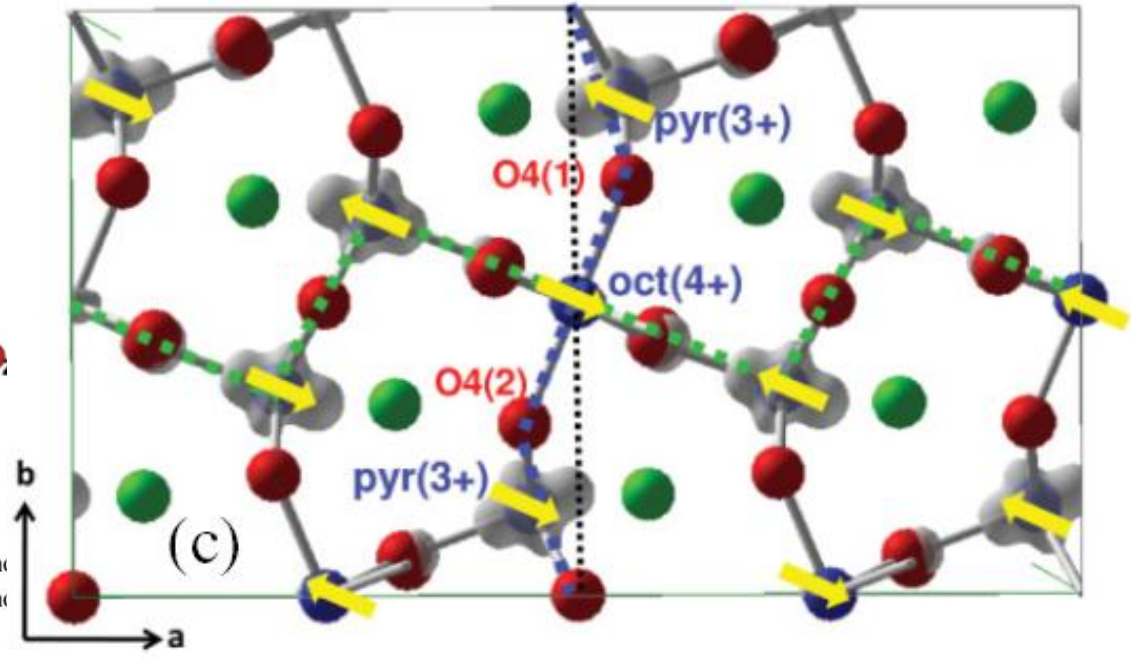

Band Gap of $TbMn_2O_5$ vs on-site U

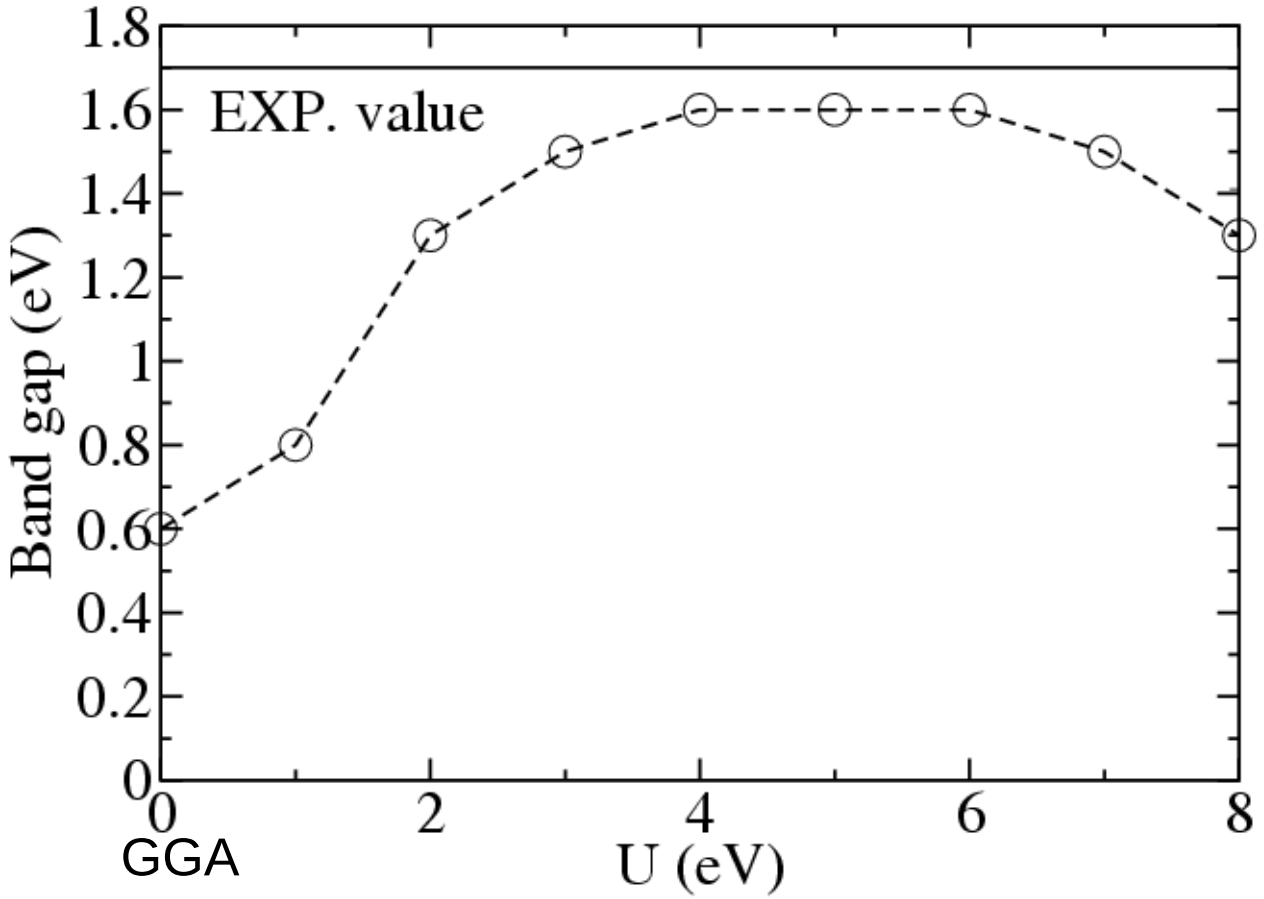

The reasonable range of U is from 4 to 6 eV.

Frustrated spin alignment along b

- : Mn3+
+ : Mn4+

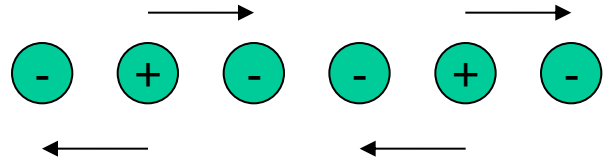

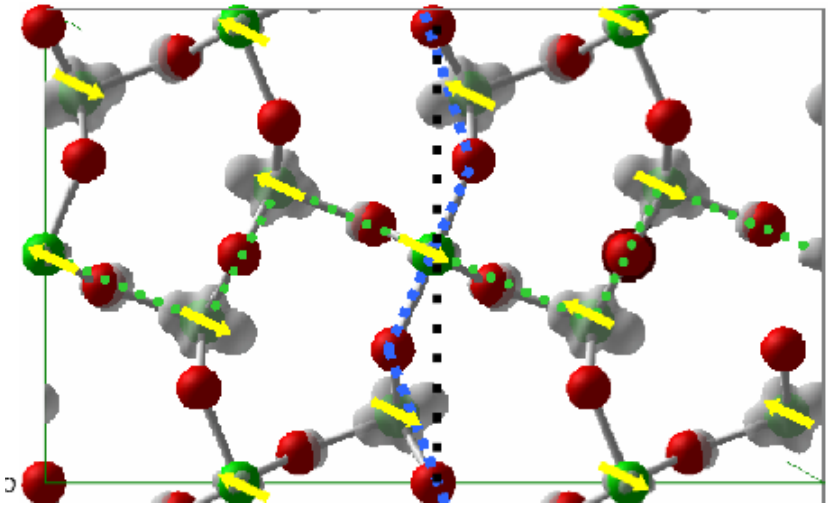

b
a

Ionic force

a

a: zero polarization

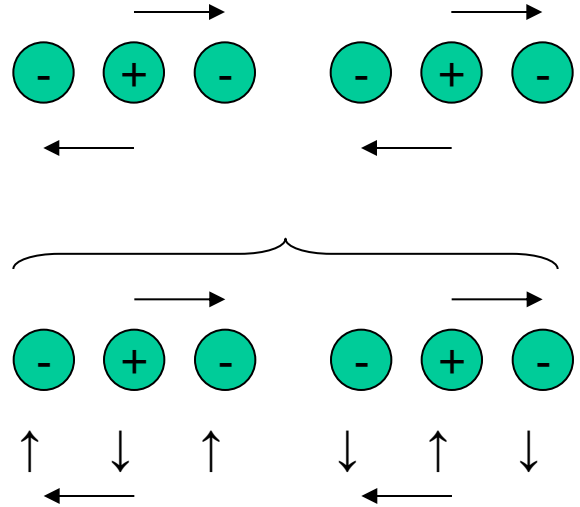

magnetostriction

b

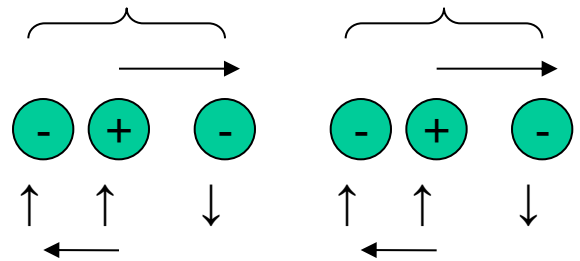

EXP : 42 nC/cm^2
GGA: 1027 nC/cm^2

Intersite exchange force (magnetostriction)

P

Polarization vs on-site U

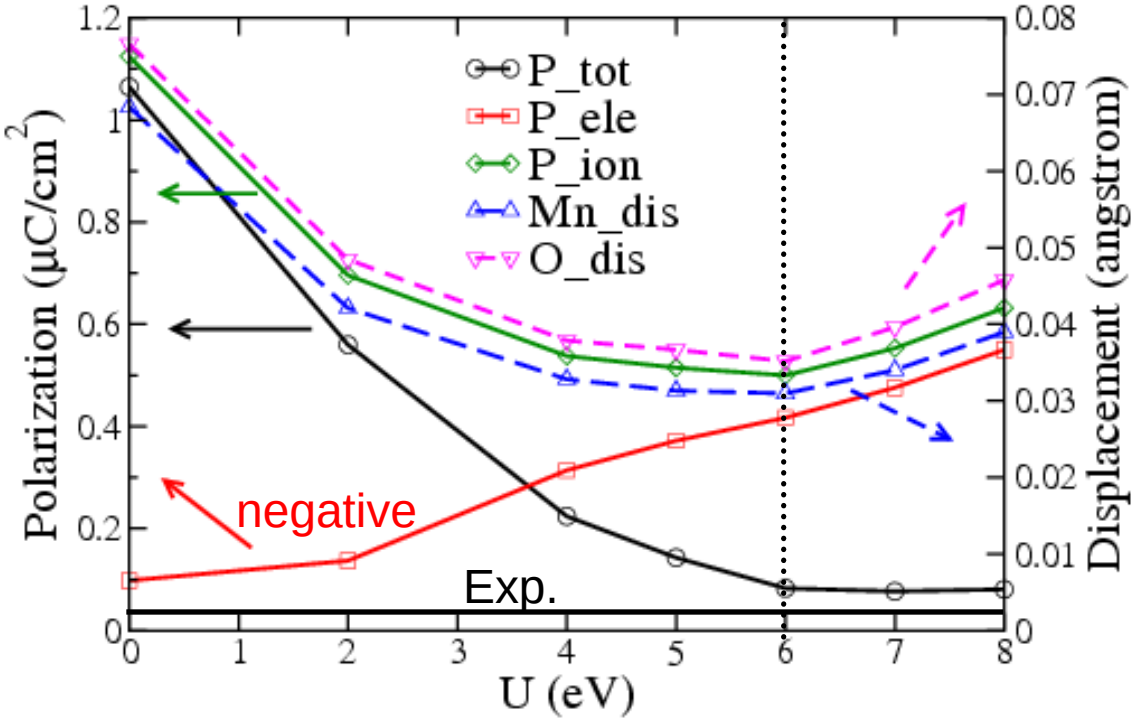

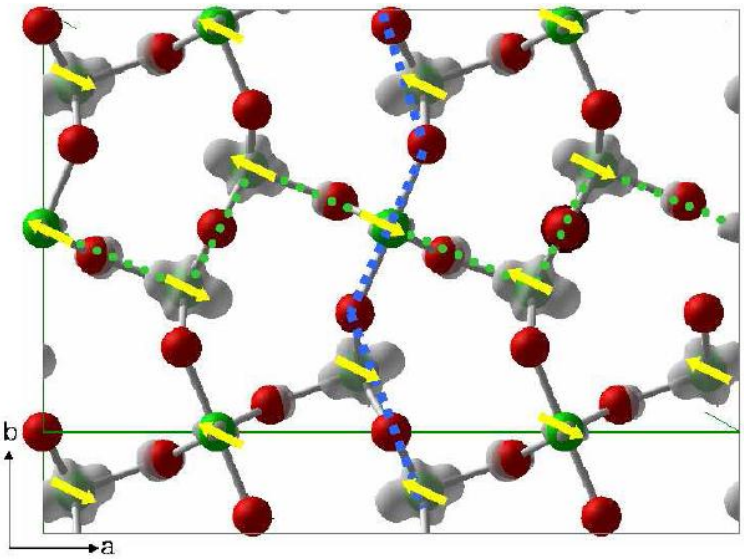

EXP： 42 nC/cm^2
U=0：1027 nC/cm^2
U=6：83 nC/cm^2

*Pele against Pion
*best U for both band gap and polarization: 6eV
*GGA: Pion>>Pele →large P
*U supress Pion and enhance Pele → small P
*spin-orbit interaction has no significant effect

Topological insulator Be2Se3 Crystal Structure

- Lattice constant
  a= 4.143 Ang.
  c= 28.63
- Space group
  R-3m (No. 166)

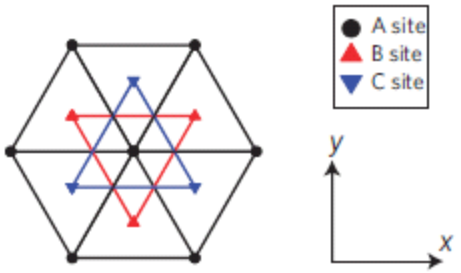

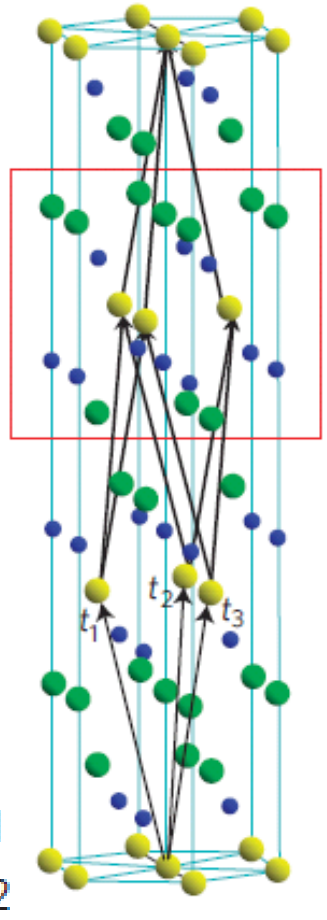

Quintuple layer

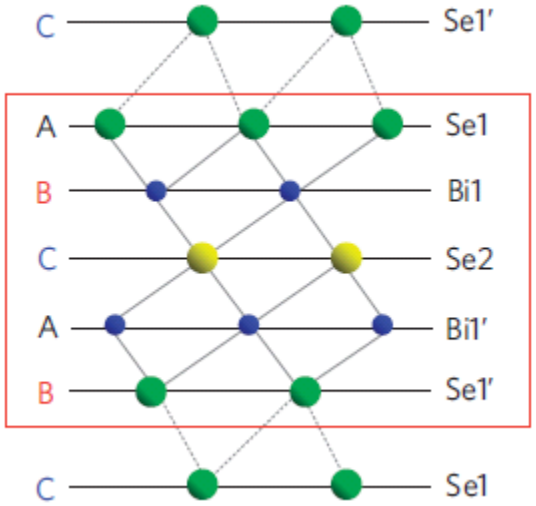

Time reversal symmetry
+spin-orbit interaction
+band inversion

Nat. Phys. **5**, 438 (2009)

insulator

Bi_2Se_3

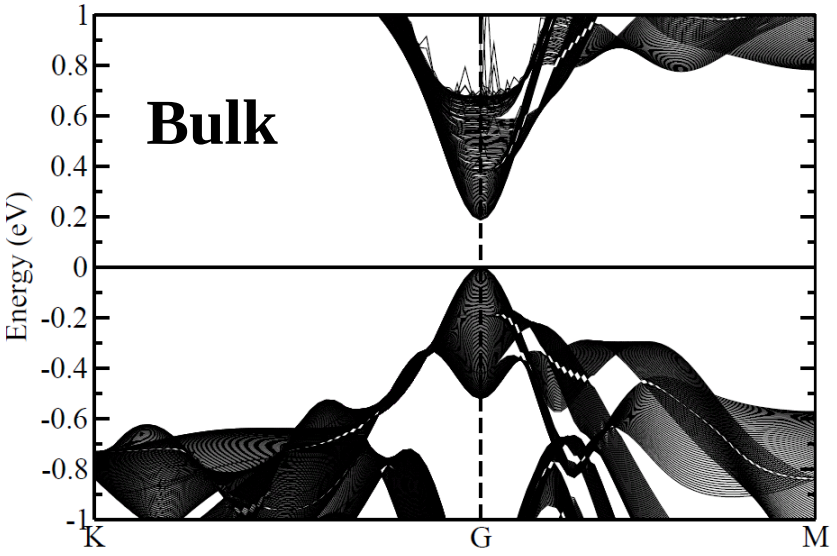

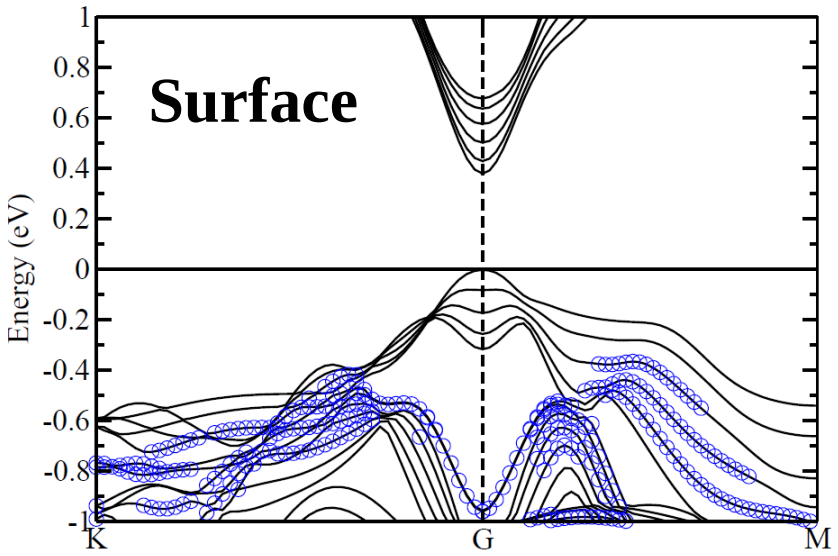

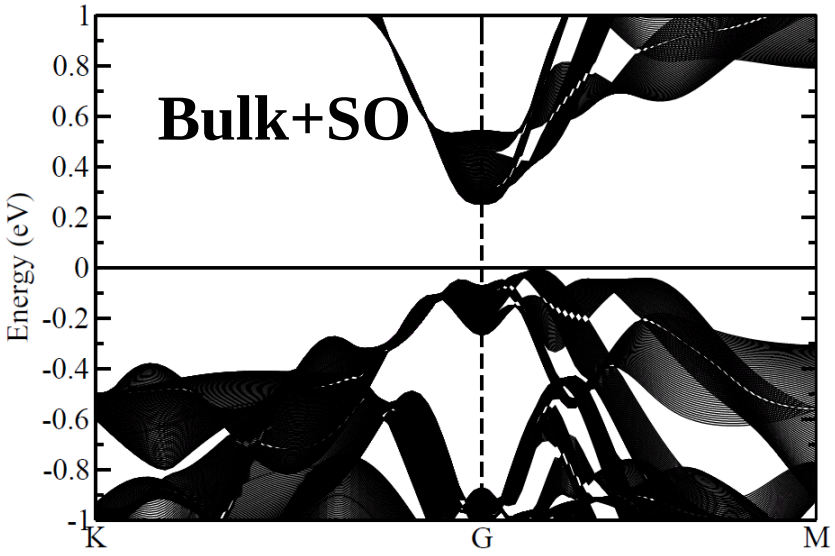

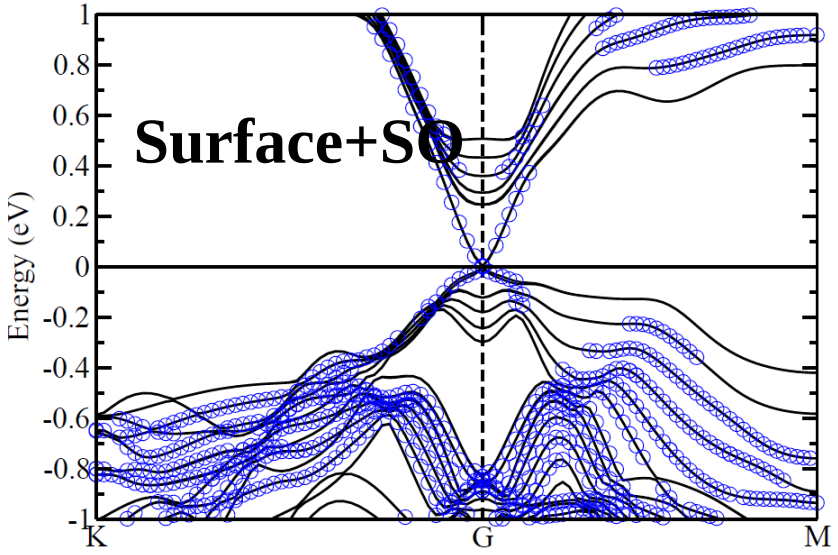

metal

Spintexture

upper cone, top surface

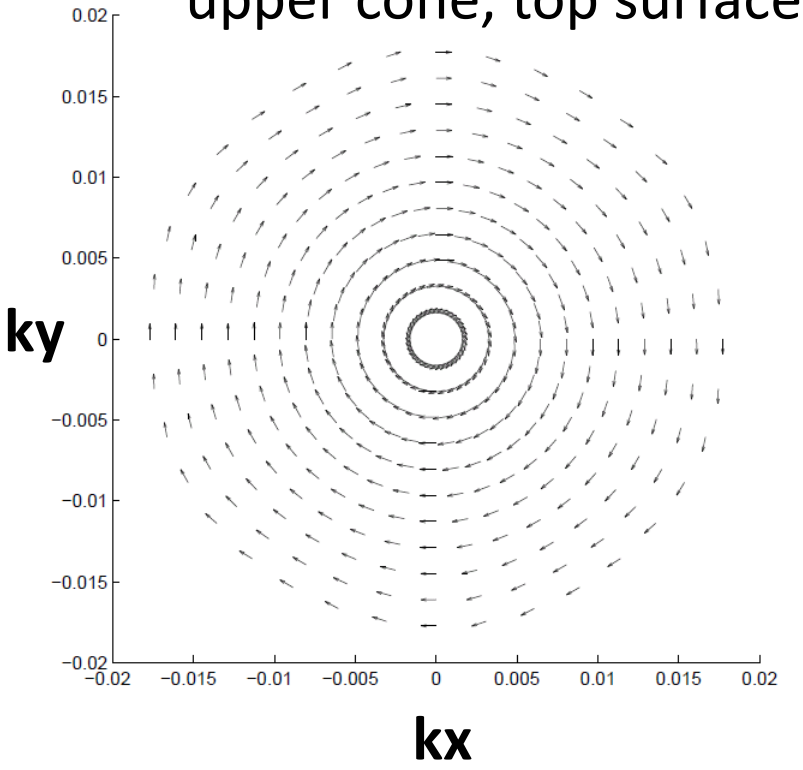

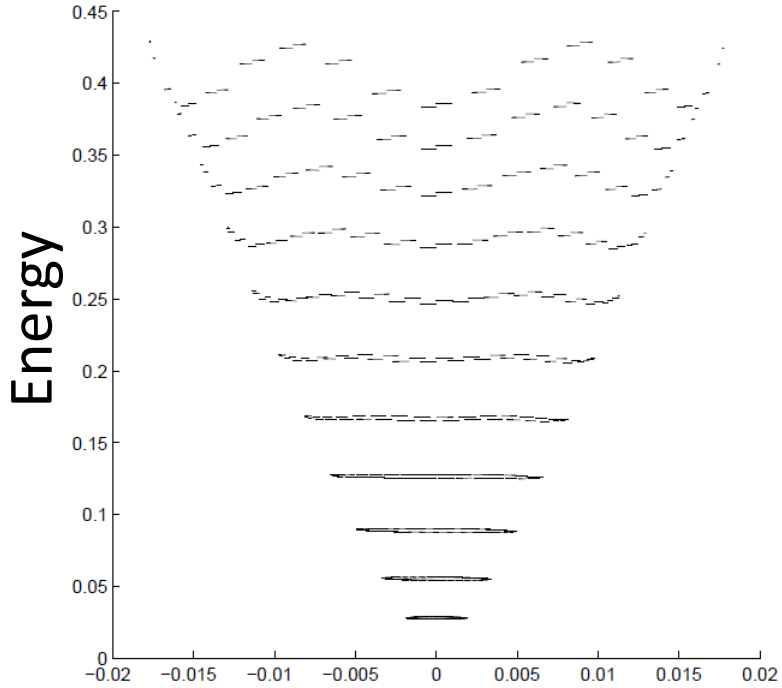

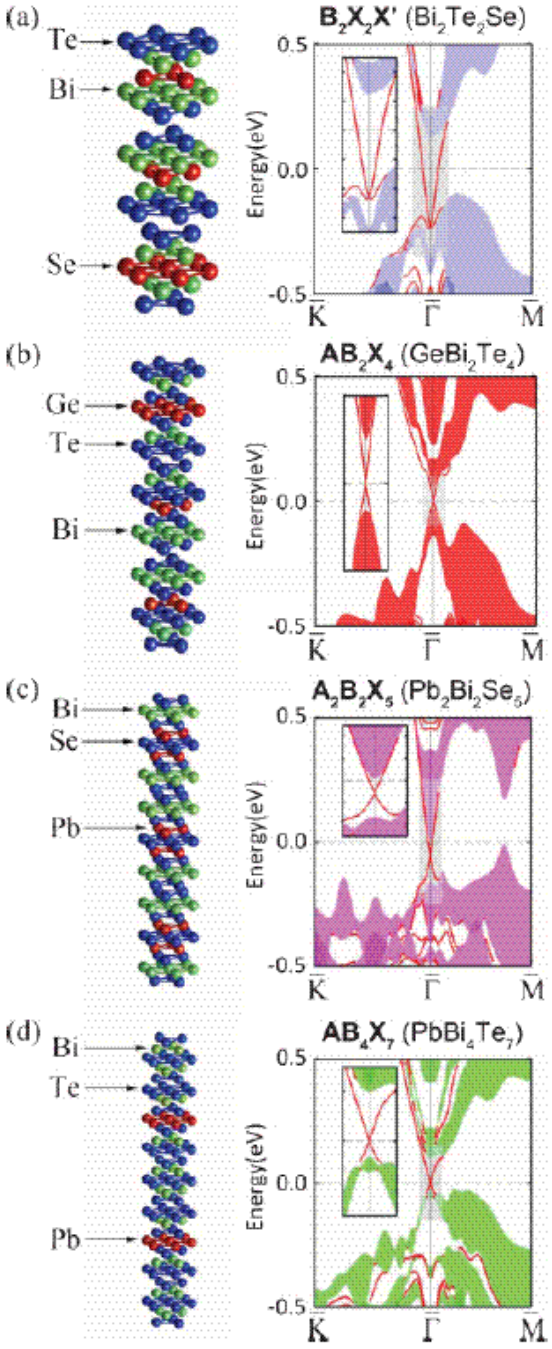
(a)
Te
Bi
Se
B_2X_2X' (Bi_2Te_2Se)
Energy(eV)
0.5
0.0
-0.5
K̄
Γ̄
M̄
(b)
Ge
Te
Bi
AB_2X_4 ($GeBi_2Te_4$)
(c)
Bi
Se
Pb
$A_2B_2X_5$ ($Pb_2Bi_2Se_5$)
(d)
Bi
Te
Pb
AB_4X_7 ($PbBi_4Te_7$)

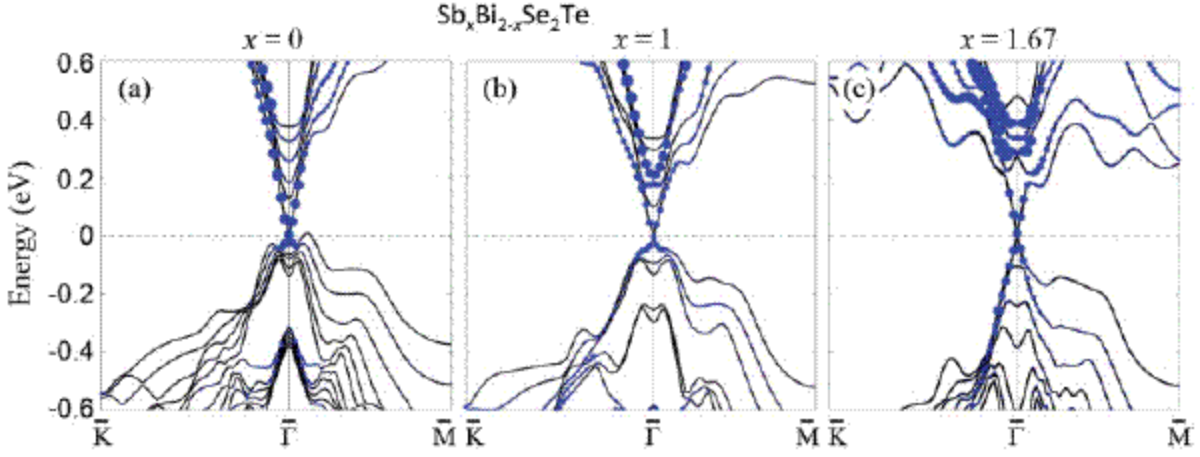
$Sb_xBi_{2-x}Se_2Te$
x = 0
x = 1
x = 1.67
(a)
(b)
(c)
Energy (eV)
0.6
0.4
0.2
0
-0.2
-0.4
-0.6
K̄
Γ̄
M̄

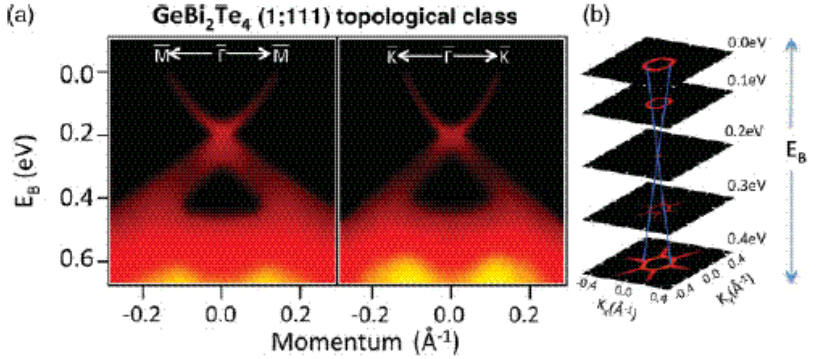
(a)
$GeBi_2Te_4$ (1;111) topological class
M̄ ← Γ̄ → M̄
K̄ ← Γ̄ → K̄
E_B (eV)
0.0
0.2
0.4
0.6
-0.2
0.0
0.2
Momentum (Å^{-1})
(b)
0.0eV
0.1eV
0.2eV
0.3eV
0.4eV
E_B

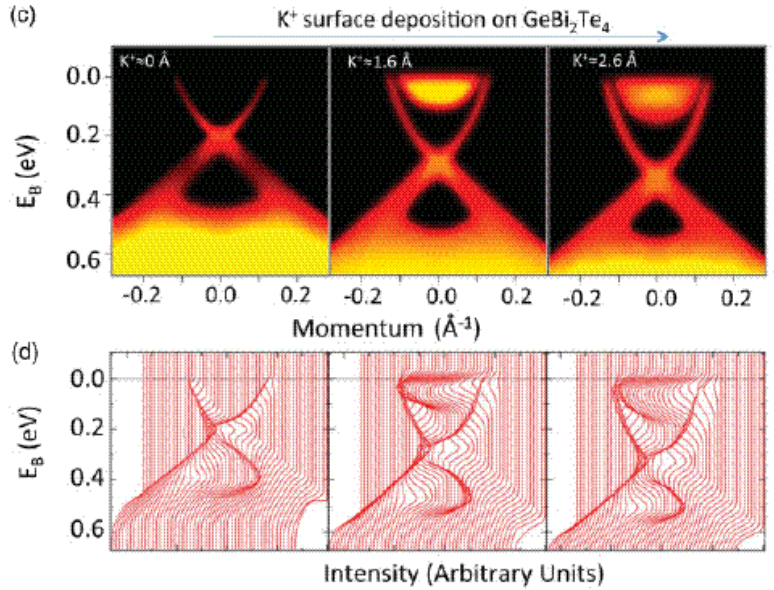
(c)
K^+ surface deposition on $GeBi_2Te_4$
K^+≈0 Å
K^+≈1.6 Å
K^+=2.6 Å
E_B (eV)
0.0
0.2
0.4
0.6
-0.2
0.0
0.2
Momentum (Å^{-1})
(d)
Intensity (Arbitrary Units)

ARPES Bi2Se3

Nat. Phys. **5**, 398 (2009)

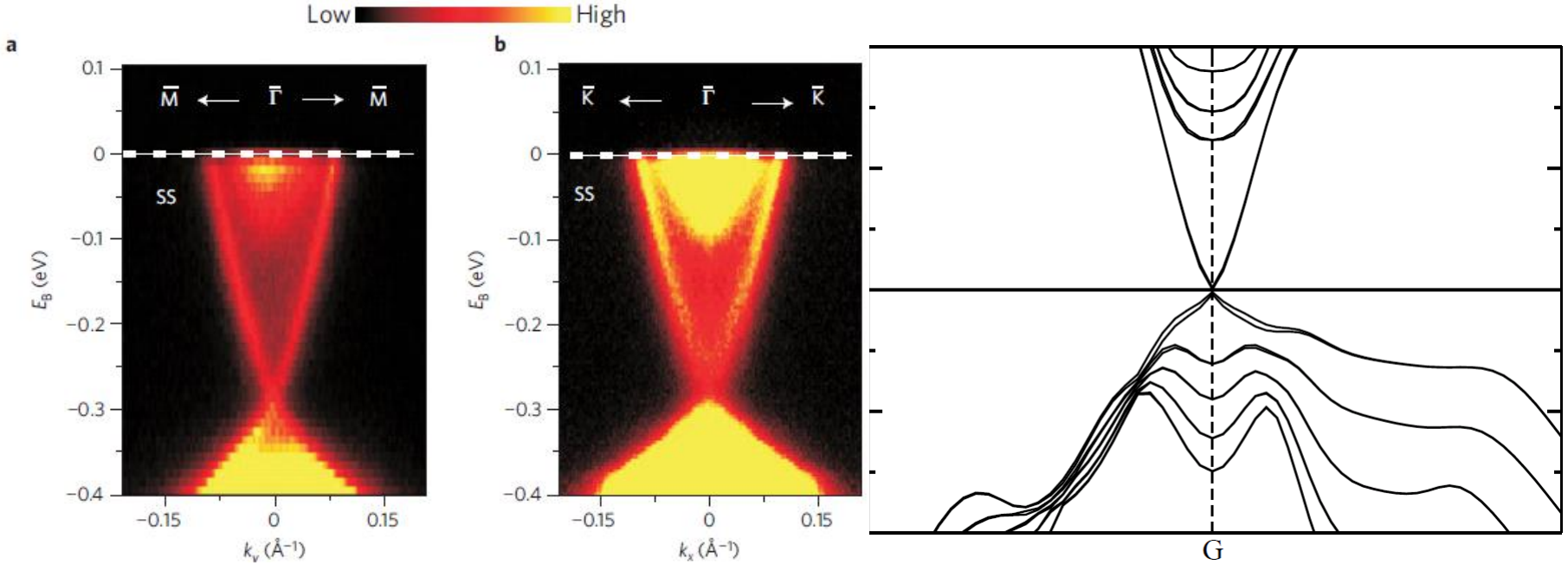

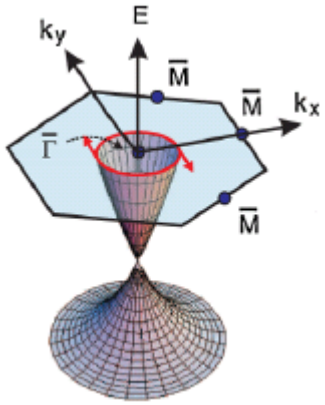

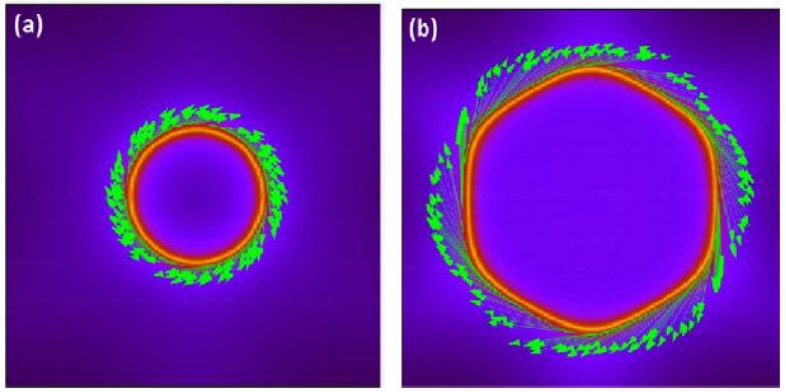

New J. Phys. **12**, 065013 (2010)

ARPES of Mn- and Zn-doped Bi2Se3

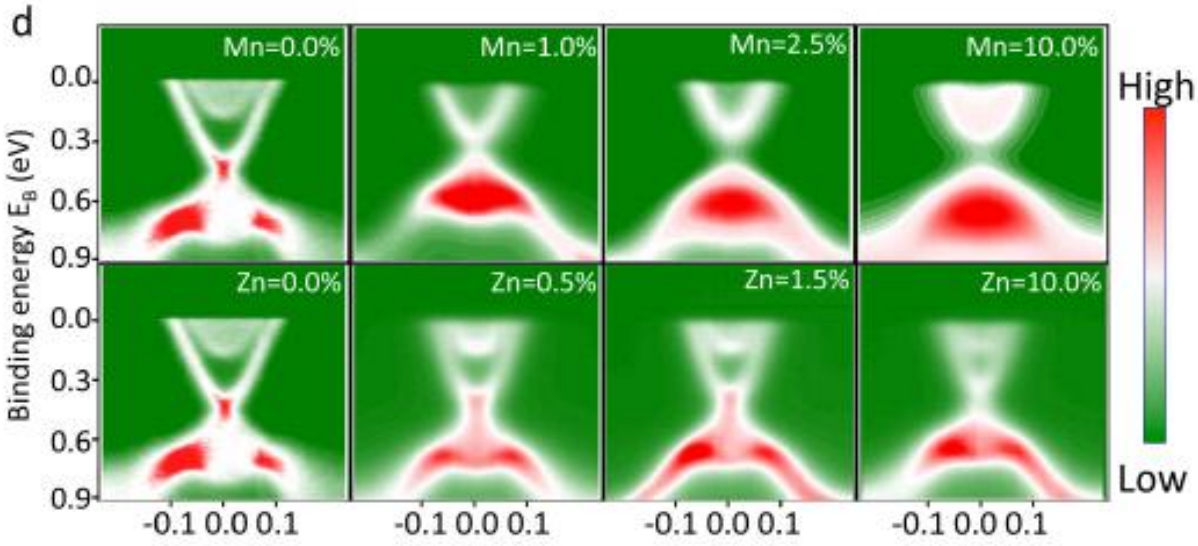

Gap open at %2.5 Mn

No noticeable change below 10% Zn

X-ray magnetic circular dichroism (XMCD):
Hysteretic response of 2.5% Mn-doped Bi2Se3
(no hysteretic response of Zn-doped cases)

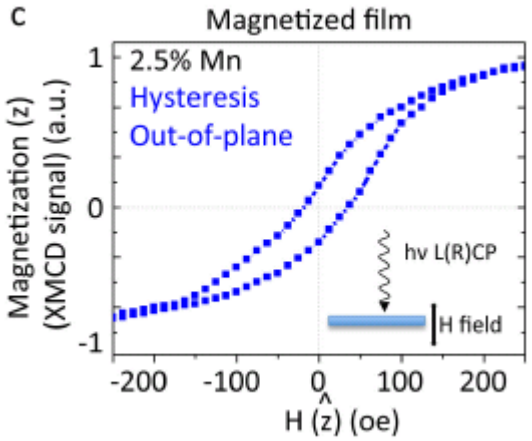

Spectral weight suppression at the Dirac point of Mn-doped Bi2Se3

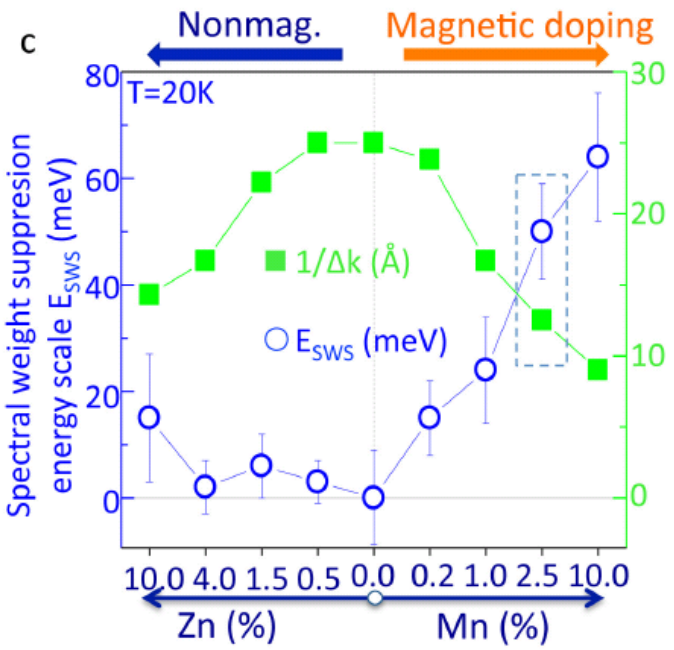

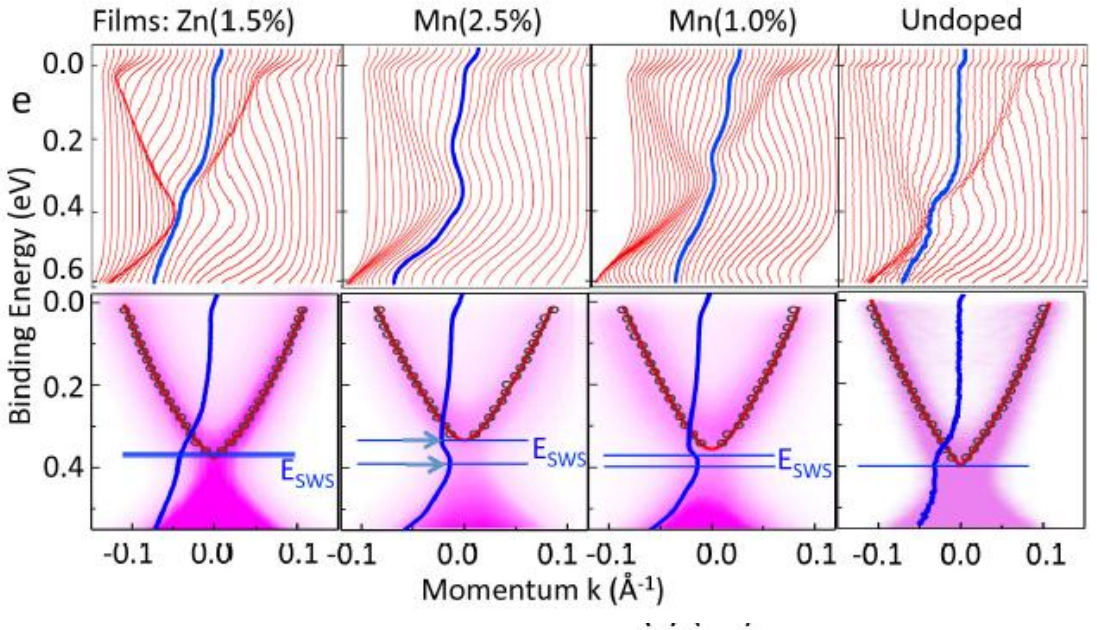

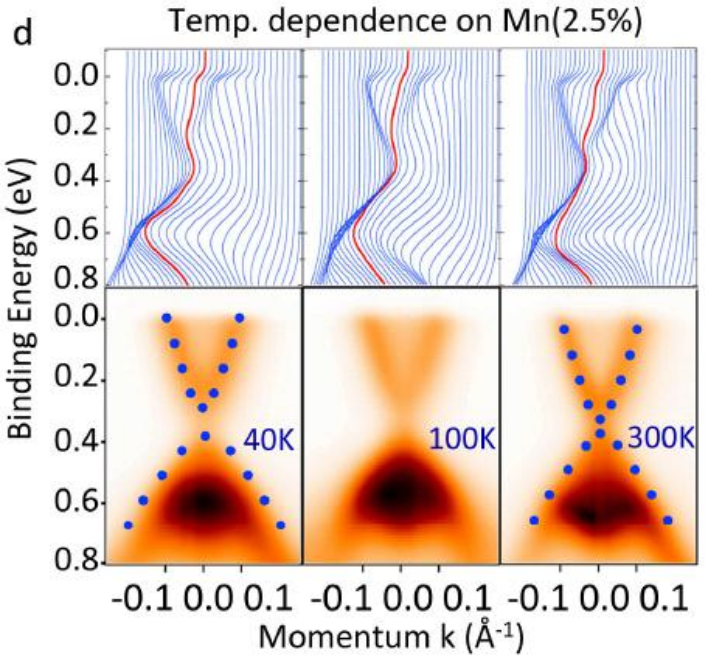

Gap suppression at high-temperature
Due to the suppressed magnetism

momentum distribution curve (MDC) of Mn-doped Bi2Se3

(from –k to +k for a given energy)

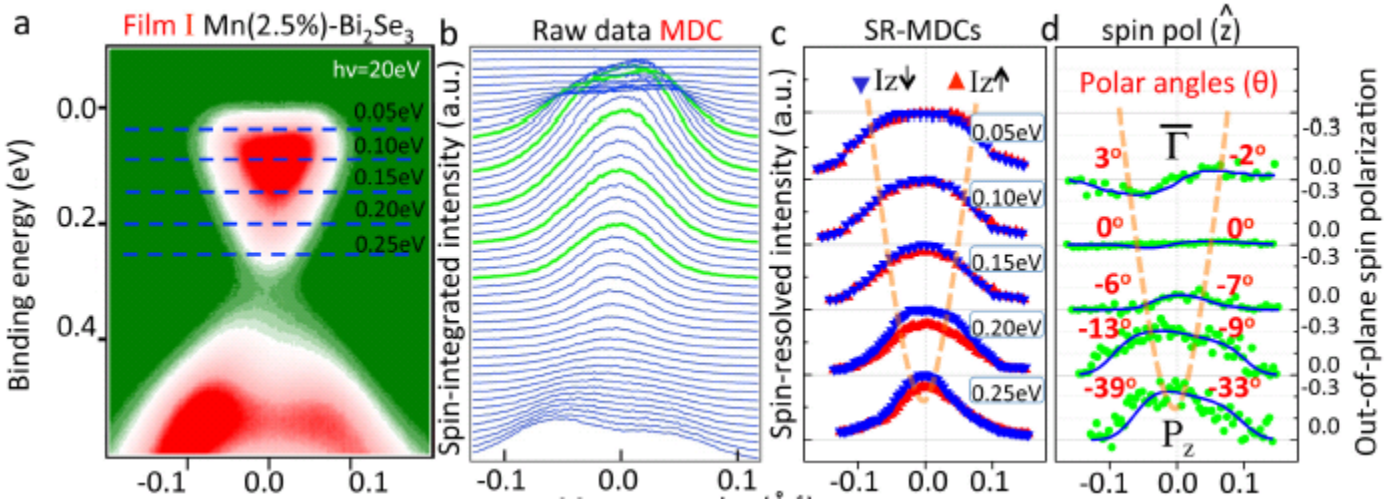

*Spin reorients to out-of-plane direction near the Dirac point (DP) with the same sign for both +k and –k, breaking the time-reversal symmetry (TRS)

*Away from the DP, the out-of-plane spin polarization is reduced with different sign for +k and –k, reserving the TRS

energy distribution curve (EDC) of Mn-doped Bi2Se3 (from –E to +E for a given momentum)

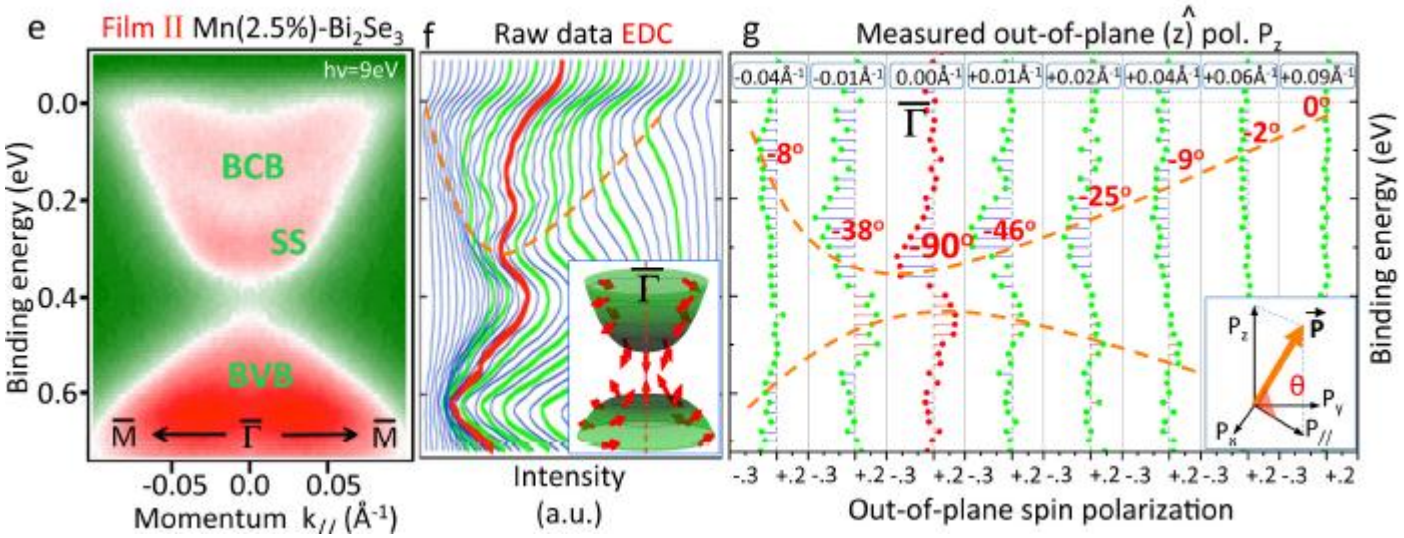

*Out-of-plane spin direction reverses for lower Dirac cone (red-line at Gamma), lifting the spin degeneracy at DP (E(k=0,↑)≠E(K=0,↓)), breaking the Kramer theory

*The out-of-plane spin polarization dies out away from the Dirac point (green lines)

energy distribution curve (EDC) of Zn-doped Bi2Se3
(from –E to +E for a given momentum)

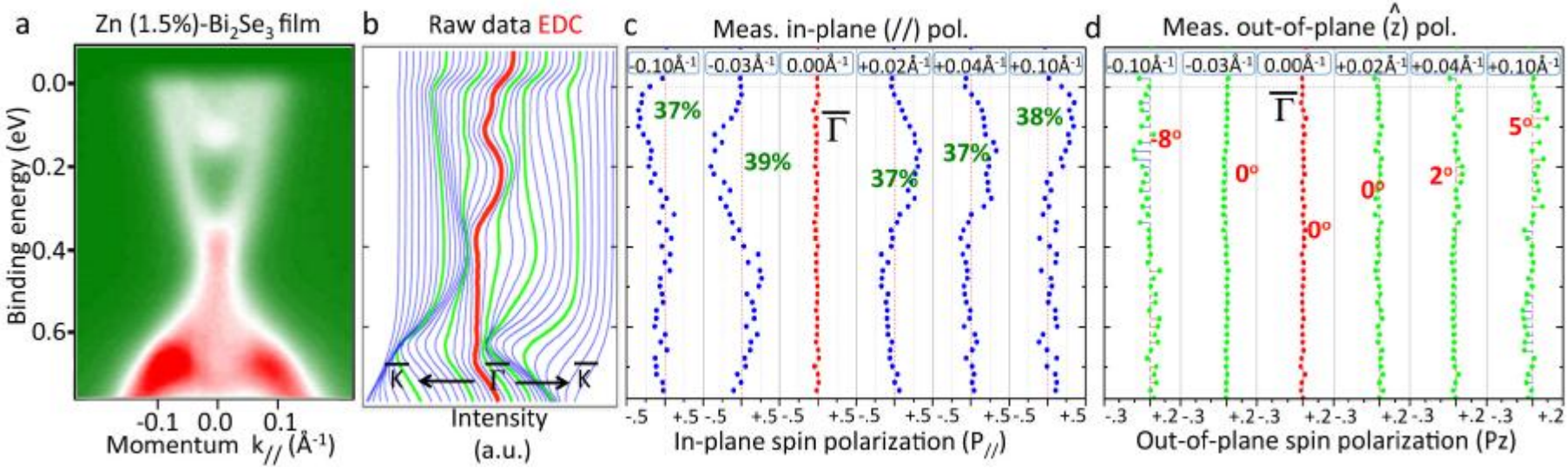

*No out-of-plane spin polarization around the Dirac point (red line at Gamma in d)

*Out-of-plane spin polarization observed away from the DP with the TRS preserved (green lines in d)

*In-plane spin polarization observed around the DP, reserving the TRS (blue lines in c) ->Zn dopants do not break the spin texture and the TRS

energy distribution curve (EDC) of 3QL Bi2Se3 (from –E to +E for a given momentum)

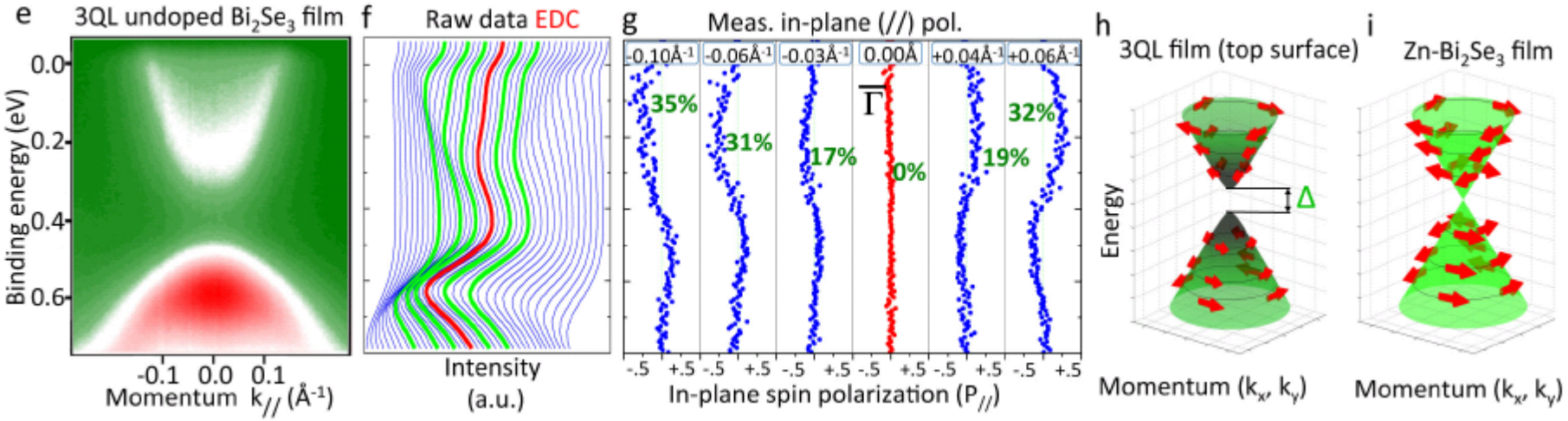

*gap opening in Bi2Se3 3QL thin film due to the top-bottom surface state interaction, irrelevant to magnatism (e)

*in-plane spin polarization (g), different sign in –k and +k, reserving the TRS

* left-handed helical spin texture in 3QL Bi2Se3 and Zn-doped Bi2Se3 (h,i)

NO2 absorption modify the Ef

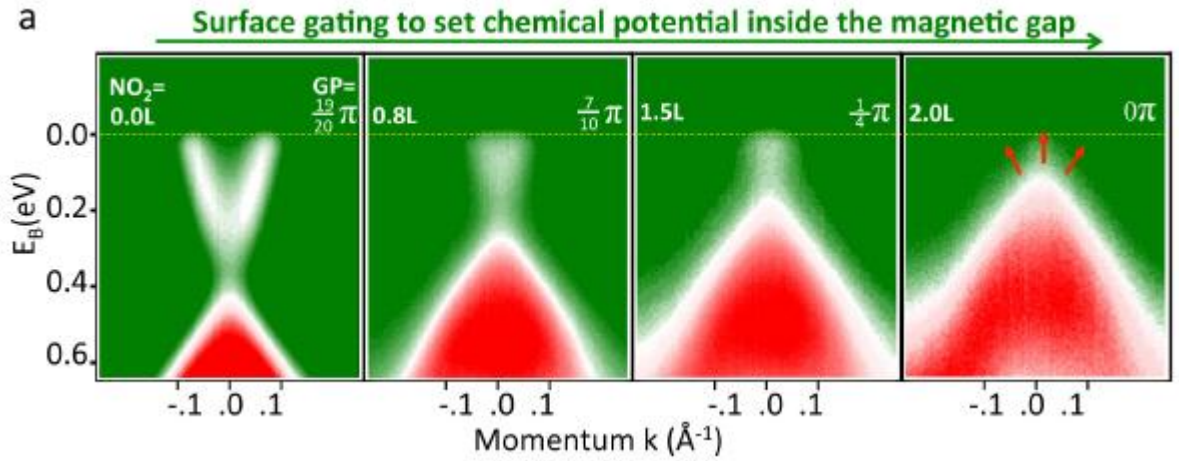

The more NO2 adsorbed (up to 2ML) the lower Ef
-> Ef can be tuned to lie inside the magnetic gap

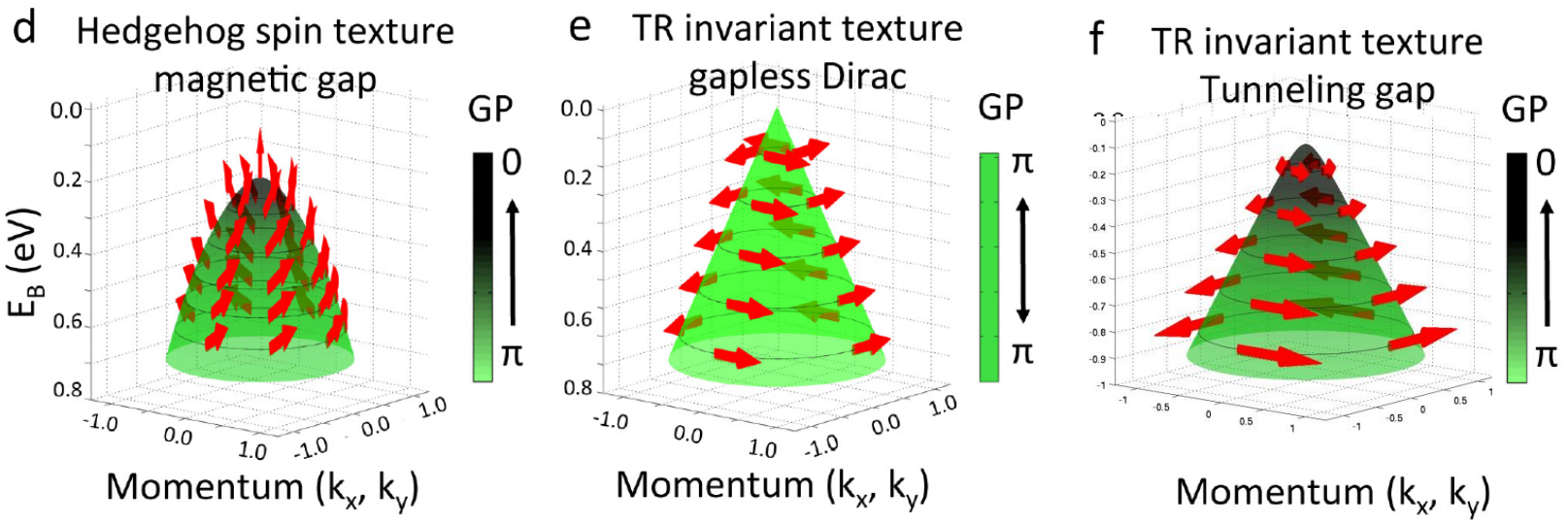

Gated silicene as a tunable source of nearly 100% spin-polarized electrons

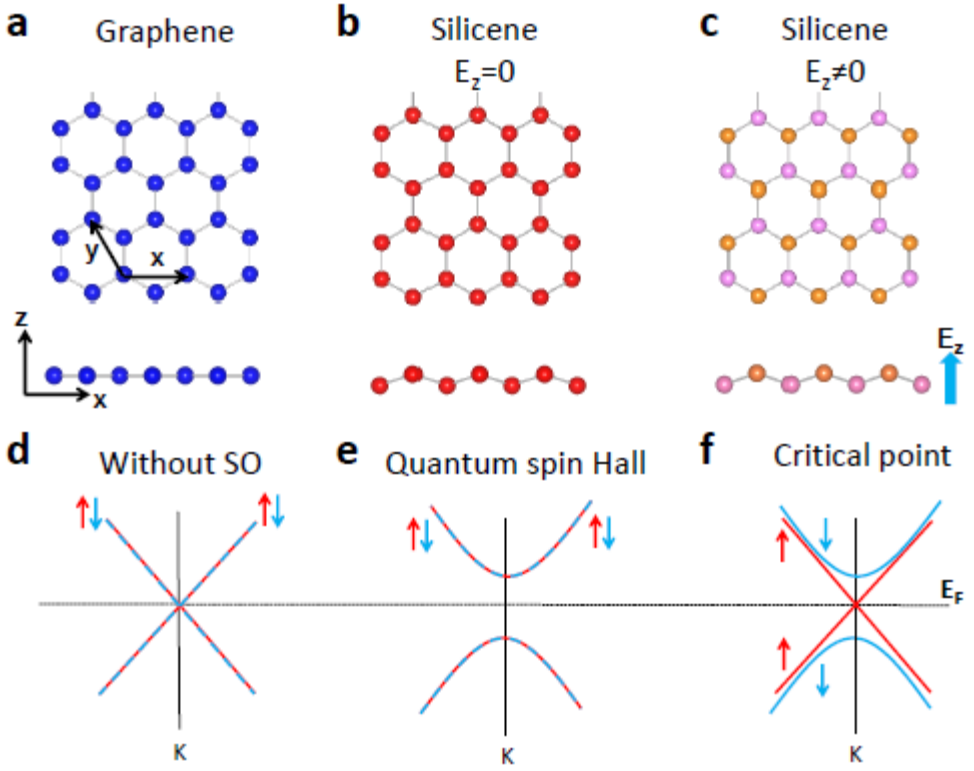

FIG. 1: The 2D honeycomb structure of (a) graphene, (b) silicene, and (c) silicene under an out-of-plane electric field. The band structure of: (d) graphene without SO; (e) silicene with SO interaction; and (f) silicene with SO interaction at the critical point of topological phase transition. The red and blue arrows indicate the spin direction.

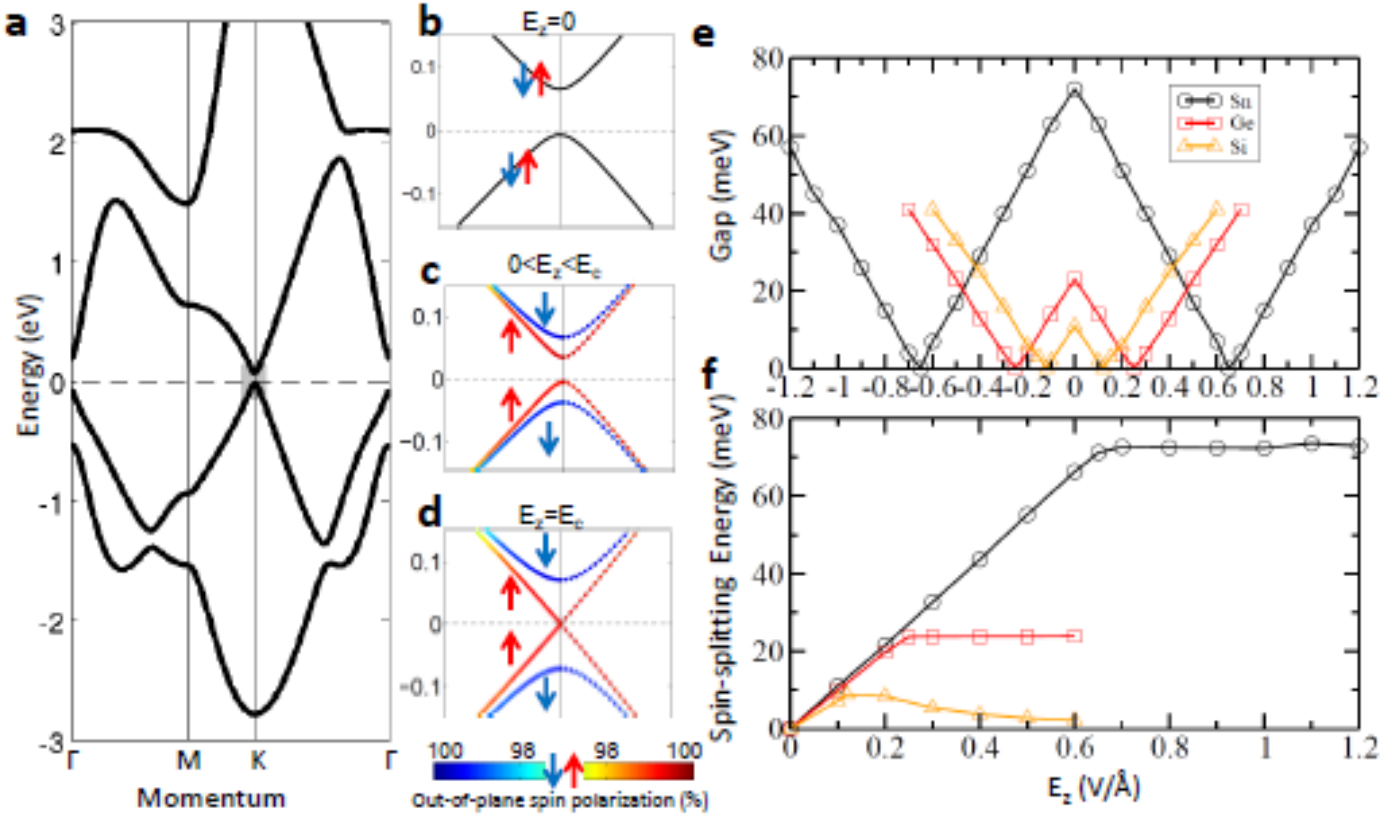

FIG. 2: (a) First-principles band structures of 2D low-buckled honeycomb structure of Sn with SO interaction. (b)-(d) are zoomed in band structures in the gray zone of (a) for E_z=0, 0<E_z<E_c, and $E_z = E_c$, respectively. Red and blue arrows indicate up and down spin, respectively. The degree of out-of-plane spin polarization is shown in color in (c) and (d). (e) Band gap evolution under electric field. (f) Spin-splitting energy at the K point as a function of E_z.

Thank you very much
for your attention